Biogeosciences Discuss., 12, 8939–9004, 2015
www.biogeosciences-discuss.net/12/8939/2015/
doi:10.5194/bgd-12-8939-2015

Biogeosciences Discussions
Open Access

The effect of warm-season precipitation on the diel cycle of the surface energy balance and carbon dioxide at a Colorado subalpine forest site

S. P. Burns[1,2], P. D. Blanken[1], A. A. Turnipseed[3], and R. K. Monson[4]

[1]Department of Geography, University of Colorado, Boulder, Colorado, USA
[2]National Center for Atmospheric Research, Boulder, Colorado, USA
[3]2B Technologies, Inc., Boulder, Colorado, USA
[4]School of Natural Resources and the Environment, University of Arizona, Tucson, Arizona, USA

Received: 15 May 2015 – Accepted: 21 May 2015 – Published: 16 June 2015

Correspondence to: S. P. Burns (sean@ucar.edu)

Published by Copernicus Publications on behalf of the European Geosciences Union.

Abstract

Precipitation changes the physical and biological characteristics of an ecosystem. Using a precipitation-based conditional sampling technique and a 14 year dataset from a 25 m micrometeorological tower in a high-elevation subalpine forest, we examined how warm-season precipitation affected the above-canopy diel cycle of wind and turbulence, net radiation R_{net}, ecosystem eddy covariance fluxes (sensible heat H, latent heat LE, and CO_2 net ecosystem exchange NEE) and vertical profiles of scalars (air temperature T_a, specific humidity q, and CO_2 dry mole fraction χ_c). This analysis allowed us to examine how precipitation modified these variables from hourly (i.e., the diel cycle) to multi-day time-scales (i.e., typical of a weather-system frontal passage).

During mid-day we found: (i) even though precipitation caused mean changes on the order of 50–70 % to R_{net}, H, and LE, the surface energy balance (SEB) was relatively insensitive to precipitation with mid-day closure values ranging between 70–80 %, and (ii) compared to a typical dry day, a day following a rainy day was characterized by increased ecosystem uptake of CO_2 (NEE increased by ≈ 10 %), enhanced evaporative cooling (mid-day LE increased by ≈ 30 W m^{-2}), and a smaller amount of sensible heat transfer (mid-day H decreased by ≈ 70 W m^{-2}). Based on the mean diel cycle, the evaporative contribution to total evapotranspiration was, on average, around 6 % in dry conditions and 20 % in wet conditions. Furthermore, increased LE lasted at least 18 h following a rain event. At night, precipitation (and accompanying clouds) reduced R_{net} and increased LE. Any effect of precipitation on the nocturnal SEB closure and NEE was overshadowed by atmospheric phenomena such as horizontal advection and decoupling that create measurement difficulties. Above-canopy mean χ_c during wet conditions was found to be about 2–3 µmol mol^{-1} larger than χ_c on dry days. This difference was fairly constant over the full diel cycle suggesting that it was due to synoptic weather patterns (different air masses and/or effects of barometric pressure). In the evening hours during wet conditions, weakly stable conditions resulted in smaller

BGD
12, 8939–9004, 2015

vertical χ_c differences compared to those in dry conditions. Finally, the effect of clouds on the timing and magnitude of daytime ecosystem fluxes is described.

1 Introduction

Forest ecosystem disturbances can be natural (e.g., wildfire, insect outbreaks) or anthropogenic (clear-cutting of forests, etc.) in origin. Warm-season precipitation is a common perturbation that changes the physical and biological properties of a forest ecosystem. The most obvious effect is the wetting of vegetation and ground surfaces which provides liquid water for evaporation and changes the surface energy partitioning between sensible heat flux H and latent heat flux LE (i.e., evapotranspiration). Such changes are important in the modeling of ecosystem process on both local and global scales (e.g., Bonan, 2008). Liquid water infiltration also changes the thermal diffusivity of the soil (Garratt, 1992; Cuenca et al., 1996; Moene and Van Dam, 2014) as well as the rain itself transporting heat into the soil (Kollet et al., 2009). Rain can also suppress the release of CO_2 from soil because of inhibited CO_2 diffusion/transport due to water-filled soil pore space (Hirano et al., 2003; Ryan and Law, 2005). The soil and the atmosphere near the ground are closely coupled, and therefore soil moisture changes also affect near-ground atmospheric properties (Betts and Ball, 1995; Pattantyús-Ábrahám and Jánosi, 2004).

Rain has been shown to cause short-lived increases in soil respiration by microorganisms (by as much as a factor of ten) in diverse ecosystems ranging from: deciduous eastern US forests (Lee et al., 2004; Savage et al., 2009), ponderosa pine plantations (Irvine and Law, 2002; Tang et al., 2005; Misson et al., 2006), California oak-savanna grasslands (Xu et al., 2004), Colorado shortgrass steppe (Munson et al., 2010; Parton et al., 2012), arid/semi-arid regions across the western US (Huxman et al., 2004; Austin et al., 2004; Ivans et al., 2006; Jenerette et al., 2008; Bowling et al., 2011), Mediterranean oak woodlands (Jarvis et al., 2007), and abandoned agricultural fields (Inglima et al., 2009). The pulse of CO_2 emitted from soil that accompanies precipitation follow-

BGD
12, 8939–9004, 2015

ing a long drought period is one aspect of the so-called Birch effect (named after H. F. Birch (1912–1982), see Jarvis et al. (2007); Borken and Matzner (2009); Unger et al. (2010) for a summary). The timing, size, and duration of the precipitation event (as well as the number of previous wet–dry cycles) all affect the magnitude of the microbial and plant/tree responses to the water entering the system. The response of soil respiration to a rain pulse typically has an exponential decay with time (Xu et al., 2004; Jenerette et al., 2008). The Birch effect is especially important for the carbon balance in arid or water-limited ecosystems where background soil respiration rates are generally low.

Net ecosystem exchange of CO_2 (NEE) is calculated from the above-canopy eddy covariance CO_2 vertical flux plus the temporal changes in the CO_2 dry mole fraction between the flux measurement-level and the ground (i.e., the CO_2 storage term). The studies listed in the previous paragraph have used a combination of eddy-covariance, soil chambers, and continuous in-situ CO_2 mixing ratio measurements to examine ecosystem responses to precipitation. Many of these studies have also shown that CO_2 pulses due to the Birch effect have an important influence on the seasonal and annual budget of NEE for that particular ecosystem (e.g., Lee et al., 2004; Jarvis et al., 2007; Parton et al., 2012). In the current study we will not be concerned with mechanistic or biological aspects of the Birch effect, but instead focus on how precipitation affects above-canopy NEE and any possible implications on the annual carbon budget.

Evaporation from wet surfaces was initially modeled by Penman (1948) using available energy (primarily net radiation), the difference between saturation vapor pressure and atmospheric vapor pressure at a given temperature (i.e., $e_s - e_d$, also known as the vapor pressure deficit, VPD), and aerodynamic resistances to formulate an expression for surface LE. The concepts by Penman were extended to include transpiration by Monteith (1965) who introduced the concept of canopy resistance (a resistance to transpiration which is in series with the aerodynamic resistance, but controlled by the leaf stomates) leading to the Penman–Monteith equation for latent heat flux over dry vegetation. Based on these formulations, the fundamental variables which are believed to control evapotranspiration are net radiation, sensible heat flux, atmospheric stabil-

BGD
12, 8939–9004, 2015

ity (which affects the aerodynamic resistances), stomatal resistance, and VPD. It has been questioned whether stomates respond to the rate of transpiration rather than VPD (e.g., Monteith, 1995). It has also been shown that stability/wind speed only has a small direct effect on transpiration (e.g., Kim et al., 2014). Since our study is focused on both evaporation and transpiration changes, we focus on the diel changes in the measured variables listed above.

Near vegetated surfaces, it is known that the atmospheric fluxes of CO_2 and water vapor are correlated to each other because the leaf stomates control both photosynthesis and transpiration (Monteith, 1965; Brutsaert, 1982; Jarvis and McNaughton, 1986; Katul et al., 2012; Wang and Dickinson, 2012). There are also temporal changes (and feedbacks) to LE related to boundary layer growth and entrainment which are summarized by van Heerwaarden et al. (2009, 2010). One of the drawbacks to the eddy covariance measurement of LE is that the contributions from the physical process of evaporation are not easily separated from the biological process of transpiration without making some assumptions of stomatal behavior (e.g., Scanlon and Kustas, 2010), using isotopic methods (e.g., Yakir and Sternberg, 2000; Williams et al., 2004; Werner et al., 2012; Jasechko et al., 2013; Berkelhammer et al., 2013), or having additional measurements, such as sap flow (e.g., Hogg et al., 1997; Oishi et al., 2008; Staudt et al., 2011) or weighing lysimeters (e.g., Grimmond et al., 1992; Rana and Katerji, 2000; Blanken et al., 2001). Another technique uses above-canopy eddy-covariance instruments for evapotranspiration coupled with sub-canopy instruments to estimate evaporation (e.g., Blanken et al., 1997; Law et al., 2000; Wilson et al., 2001; Staudt et al., 2011); this method, however, can have issues with varying flux footprint sizes (Misson et al., 2007). An accurate way to separate transpiration and evaporation has been a goal of the ecosystem-measurement community for many years.

Numerous studies have looked at the annual and interannual relationship between precipitation, water fluxes and NEE at the climate scale (Aubinet et al., 2000; Wilson et al., 2001; Law et al., 2002; Malhi et al., 2002; Thomas et al., 2009; Hu et al., 2010a; Polley et al., 2010, and many others). However, a comprehensive examination of the

BGD
12, 8939–9004, 2015

effect of precipitation on ecosystem-scale eddy covariance fluxes at the diel (i.e., hourly or "weather-front") time scale is lacking.

Our study uses fourteen years of data from a high-elevation subalpine forest AmeriFlux site to explore how warm-season rain events (defined as a daily precipitation total greater than 3 mm) change the mean meteorological variables (horizontal wind speed U, air temperature T_a and specific humidity q), the surface energy fluxes (latent and sensible heat), and carbon dioxide (both CO_2 mole fraction and NEE) over the diel cycle. From this analysis we can evaluate both the magnitude and timing of how the energy balance terms and NEE are modified by the presence of rainwater in the soil and on the vegetation. Precipitation is also closely linked to changes in air temperature and humidity as weather fronts and storm systems pass by the site. Since NEE and the energy fluxes depend on meteorological variables such as net radiation, air temperature and VPD, it can be difficult to separate out the effect of precipitation vs. other environmental changes (Turnipseed et al., 2009; Riveros-Iregui et al., 2011). To estimate the atmospheric stability, we use the bulk Richardson number (Ri_b) calculated with sensors near the ground and above the canopy.

Though the primary goal of our study is to quantify how precipitation modifies the warm-season mean diel cycle of the measured scalars and fluxes, a secondary goal is to present the 14 year mean and interannual variability of the energy fluxes and NEE measured at the Niwot Ridge Subalpine Forest AmeriFlux site. These results will serve as an update to the original set of papers (e.g., Monson et al., 2002; Turnipseed et al., 2002) that examined the ecosystem fluxes from the Niwot Ridge AmeriFlux site over ten years ago and were based on two years of measurements.

BGD
12, 8939–9004, 2015

2 Data and methods

2.1 Site description

Our study uses data from the Niwot Ridge Subalpine Forest AmeriFlux site (site US-NR1, more information available at http://ameriflux.lbl.gov) located in the Rocky Mountains about 8 km east of the Continental Divide. The US-NR1 measurements started in November 1998. The site is on the side of an ancient moraine with granitic-rocky-podzolic soil (typically classified as a loamy sand in dry locations) overlain by a shallow layer (≈ 10 cm) of organic material (Marr, 1961; Scott-Denton et al., 2003). The subalpine forest near the tower was established in the early 1900s following logging operations, and is primarily composed of subalpine fir (*Abies lasiocarpa* var. *bifolia*) and Englemann spruce (*Picea engelmannii*) to the west with lodgepole pine (*Pinus contorta*) to the east. Smaller patches of aspen (*Populus tremuloides*) and limber pine (*Pinus flexilis*) are also present. The tree density near the US-NR1 Tower is around 4000 trees ha^{-1} with a leaf area index (LAI) of 3.8–4.2 $m^2\,m^{-2}$ and tree heights of 12–13 m (Turnipseed et al., 2002; Monson et al., 2010). Recent analysis of tree ring cores near the US-NR1 tower has revealed a significant presence of remnant trees which are older (over 200 years old) and larger than the trees that became established after logging in the early 1900s (R. Alexander, F. Babst, and D. J. P. Moore, University of Arizona, unpublished data).

At the US-NR1 subalpine forest, ecosystem processes are closely linked to the presence of snow (Knowles et al., 2014), which typically arrives in October or November, reaches a maximum depth in early April (snow water equivalent (SWE) ≈ 30 cm), and melts by early June. Sometime in March or April, the snowpack becomes isothermal (Burns et al., 2013) and liquid water becomes available in the soil, which initiates the photosynthetic uptake of CO_2 by the forest (Monson et al., 2005). The long-term mean annual precipitation at the site is around 800 mm with about 40 % of the total from warm-season rain, which typically occurs every 2–4 days and has an average daily total of around 4 mm (Hu et al., 2010a). According to the Köppen–Geiger climate clas-

BGD
12, 8939–9004, 2015

sification system (Kottek et al., 2006) the site is type Dfc which corresponds to a cold, snowy/moist continental climate with precipitation spread fairly evenly throughout the year. The forest could also be classified as climate type H which is sometimes used for mountain locations (Greenland, 2005). The summer precipitation timing is primarily controlled by the mountain-plain atmospheric dynamics and thus usually occurs in the afternoon when upslope flows trigger convective thunderstorms (Brazel and Brazel, 1983; Parrish et al., 1990; Whiteman, 2000; Turnipseed et al., 2004; Burns et al., 2011; Zardi and Whiteman, 2013).

2.2 Surface energy balance, measurements, and data details

The terms in the surface energy balance (SEB) are,

$$R_{\text{net}} - G_z - S_{\text{soil}} - S_{\text{canopy}} = H + \text{LE} + E_{\text{adv}}, \quad (1)$$

where R_{net} is net radiation, G_z is soil heat flux measured at depth z, and the two storage terms account for the heat stored in the soil (S_{soil}) and in the biomass and airspace between the ground and the turbulent flux measurement level (S_{canopy}). All terms in Eq. (1) have units of W m^{-2}. Positive R_{net} indicates radiative warming of the surface, whereas a positive sign for the other terms in Eq. (1) indicate surface cooling. S_{canopy} and S_{soil} are typically less than 10 % of R_{net} (Oncley et al., 2007). The horizontal advection of heat and water vapor (E_{adv}) requires spatially distributed measurements, and is thought to be a primary reason that Eq. (1) does not balance at most flux sites (Leuning et al., 2012). The heat flux at the soil surface (G) was determined from G_z with 4–5 soil heat flux plates (REBS, model HFT-1) dispersed near the tower at a depth of 8–10 cm. Turnipseed et al. (2002) showed that the storage terms and G_z at US-NR1 were small (less than 8 % of R_{net}). Therefore, we neglect S_{canopy} and S_{soil} and assume the surface heat flux is close to our measured soil heat flux (i.e., $G \approx G_z$). In our discussions, the simple SEB closure fraction refers to the ratio of the sum of the turbulent fluxes to the available energy, i.e., $(H + \text{LE})/(R_{\text{net}} - G)$.

BGD
12, 8939–9004, 2015

R_{net} was measured at 25 m above ground level (a.g.l.) with both a net (REBS, model Q-7.1) and four-component (Kipp and Zonen, model CNR1) radiometer. R_{net} from the Q-7.1 sensor is about 15 % closer to closing the SEB than with the CNR1 sensor (Turnipseed et al., 2002; Burns et al., 2012). Since the Q-7.1 radiometer operated during the entire 14 year period, it is the primary R_{net} sensor in our study. The turbulent fluxes H and LE were measured at 21.5 m a.g.l. using standard eddy covariance flux data-processing techniques (e.g., Aubinet et al., 2012) and instrumentation (a 3-D sonic anemometer (Campbell Scientific, model CSAT3), krypton hygrometer (Campbell Scientific, model KH2O), and closed-path infrared gas analyzer (IRGA; LI-COR, model LI-6262)). Further details on the specific instrumentation and data-processing techniques are provided elsewhere (Monson et al., 2002; Turnipseed et al., 2002, 2003; Burns et al., 2013). Additional measurements used in our study are described in Appendix A1 while further details about updates to the US-NR1 flux calculations are in Appendix A2.

Turnipseed et al. (2002) studied the energy balance at the US-NR1 site and found that during the daytime the sum of the turbulent fluxes accounts for around 85 % of the radiative energy input into the forest. At night, under moderate turbulent conditions, simple SEB closure was comparable to the daytime; however, when the night-time conditions were either calm or extremely turbulent, H and LE only accounted for 20–60 % of the net longwave radiative flux. Burns et al. (2012) has recently shown that the lack of SEB closure for wind speeds larger than around 8 m s^{-1} was, at least partly, due to an issue with the CSAT3 sonic anemometer firmware. In the summer at US-NR1, wind speeds are rarely larger than 8 m s^{-1} so the empirical correction for H was not used in our study. When the winds are light (below about 3–4 m s^{-1}), horizontal advection is believed to be the primary reason for the lack of SEB closure.

2.3 Analysis methods

Precipitation is notoriously difficult to study because of its intermittent, binary nature (e.g., it will often start, stop, re-start, and falls with varying intensity) which leads to

BGD
12, 8939–9004, 2015

non-normal statistical properties (e.g., Zawadzki, 1973). To study the impact of rain, we followed a methodology similar to that of Turnipseed et al. (2009) and tagged days when the daily rainfall exceeded 3 mm as "wet" days. Table 1 shows the number of wet days for each year and warm-season month within our study. The choice to use 3 mm as the wet-day criteria was a balance between effectively capturing the effect of precipitation and providing enough wet periods to improve the wet-day statistics. Diel patterns for "dry days following a dry day" (designated as Dry1 days), "wet days following a dry day" (designated Wet1 days), "wet days following a wet day" (designated Wet2 days), and "dry days following a wet day" (designated Dry2 days) were analyzed to determine the effect of a precipitation on the weather and climate as well as the fluxes. If the term "wet days" is used it includes both Wet1 and Wet2 days whereas the term "dry days" includes both Dry1 and Dry2 days. In addition to these categories, we further separated the Dry1 days into sunny (Dry1-Clear) and cloudy (Dry1-Cloudy) days. These techniques are similar to the clustering analysis used by Berkelhammer et al. (2013).

Since not every variable was continuously measured for all 14 years, some variables were necessarily analyzed over shorter periods than others. A summary of the variables studied, the number of days each variable falls into each precipitation category, and gap-filling statistics of selected variables is provided in Table 2. Unless noted otherwise, the data analysis used in our study are based on 30 min statistics.

In addition to analyzing the mean diel cycle, we also examined the day-to-day variability in the diel cycle by calculating the standard deviation of the 30 min data within each composited time-of-day bin. This statistic will be designated the SD-Bin or variability in our discussion and plots. To further quantify and summarize the main results of our analysis, the diel cycle was broken up into three distinct periods: mid-day (10:00–14:00 MST), late evening (19:00–23:00 MST), and nighttime (00:00–04:00 MST). Motivation for breaking up the night into two distinct periods is provided by Burns et al. (2011) who showed that the variability of the turbulence activity (expressed by the SD-Bin of the standard deviation of the vertical wind) increased by about a factor of two at

BGD
12, 8939–9004, 2015

around 23:00 MST (see their Fig. 4d). Other flux sites with sloped terrain have shown distinct differences in the CO_2 storage before and after midnight (e.g., Aubinet et al., 2005) which provides additional motivation for separating the night into two periods.

Additional information related to the diel cycle was provided by estimating the top of the atmosphere incoming solar radiation $(Q^{\downarrow}_{SW})_{TOA}$. The sun position was calculated for the US-NR1 tower latitude and longitude with the SEA-MAT Air-Sea toolbox (Woods Hole Oceanographic Institution, 2013) which uses algorithms based on the 1978 edition of the Almanac for Computers (Nautical Almanac Office, U. S. Naval Observatory).

In order to select the warm-season period, the smoothed seasonal cycle of NEE and the turbulent energy fluxes were calculated using a 20 day mean sliding window applied to the 30 min data. Smoothing removes the effect of large-scale weather patterns (and precipitation) which typically have a period of 4–7 days. Interannual variability was calculated by taking the standard deviation among the 14 yearly smoothed time series. Since our interest is in the diel cycle, these statistics were determined for mid-day (10:00–14:00 MST), nighttime (00:00–04:00 MST), and the full (24 h) time series.

The ecosystem respiration R_{eco} was estimated for each 30 min time period based on measured nocturnal NEE (both with and without the u_* filter applied), as well as two flux-partitioning algorithms that separate NEE into R_{eco} and gross primary productivity GPP (Stoy et al., 2006). One algorithm takes into account the seasonal temperature-dependence of R_{eco} (Reichstein et al., 2005), and the other uses light-response curves (Lasslop et al., 2010). Reichstein and Lasslop R_{eco} were calculated with on-line flux-partitioning software (Max Planck Institute for Biogeochemistry, 2013). Further discussion of partitioning NEE at the US-NR1 site is provided elsewhere (Zobitz et al., 2008; Bowling et al., 2014).

Near the ground, the bulk Richardson number Ri_b is often used to characterize stability. Large negative Ri_b indicates unstable "free convection" conditions and large positive Ri_b indicates strong stability (e.g., Kaimal and Finnigan, 1994). In more stable conditions, less mixing is expected and larger vertical scalar gradients should exist (e.g., Schaeffer et al., 2008a; Burns et al., 2011). We calculated Ri_b between the highest

BGD
12, 8939–9004, 2015

($z_2 = 21.5$ m, around twice canopy height) and lowest ($z_1 = 2$ m) measurement level using:

$$\mathrm{Ri_b} = \frac{g}{\overline{T}_a} \frac{(\theta_2 - \theta_1)(z_2 - z_1)}{U^2}, \quad (2)$$

where g is acceleration due to gravity, $\overline{T}_a$ is the average air temperature of the layer, θ is potential temperature, and U is the above-canopy horizontal vectorial mean wind speed (i.e., $U = (u^2 + v^2)^{1/2}$ where u and v are the streamwise and crosswise planar-fit horizontal wind components). We did not use U near the ground because this level is deep within the canopy where U is small (less than 0.5 m s^{-1}) due to the momentum absorbed by the needles, branches and boles of the trees. In this respect, the shear-generated turbulence is related to above-canopy wind speed whereas the buoyancy is related to the temperature difference between near the ground and the overlying air. Because $\mathrm{Ri_b}$ is a ratio of two variables, it can become less useful when either the numerator or denominator becomes very small.

3 Results and discussion

3.1 Typical seasonal cycle and variability

We chose to define the start of the warm-season as the date when diurnal changes in the soil temperature first occurred (i.e., the date of near-complete snowpack ablation). For the 14 years of our study, the warm-season start dates ranged from mid-May to mid-June with an average start date of around 1 June (as shown in Fig. 1a and listed in Table 1). Though snow can occur during this period, it is a rare event and usually melts quickly. The start of the growing-season (based on NEE, as described in Hu et al., 2010a) typically preceded the start of the warm-season by 2–4 weeks (Fig. 1a). The warm-season start date was also around the time that the volumetric

BGD
12, 8939–9004, 2015

soil moisture content (VWC) reached a maximum (Fig. 1b), and the month following the disappearance of the snowpack was usually when the soil dried out (though there were exceptions, such as 2004). In the warm-season, large precipitation events led to a sharp increase in VWC followed by a gradual return (over several days or weeks) to drier soil conditions. We chose 30 September as the end of the warm-season for reasons described below.

The typical smoothed seasonal cycles of above-canopy NEE, LE and *H* are shown in Fig. 2a. For NEE, the dormant period (i.e., when the forest was inactive) was exemplified by almost no difference between the daytime and nighttime NEE, which lasted from roughly early November to mid-April. When daytime NEE switches from positive to negative, it indicates the start of the growing season. The snowmelt period exhibited strong CO_2 uptake because soil respiration was suppressed due to low soil temperature (Fig. 2a). In February–March, daytime *H* reached a maximum because net radiation increased and transpiration was small. Nighttime *H* stayed at around $-50\,W\,m^{-2}$ throughout the entire year. One might expect nocturnal *H* in winter to be different than summer, but in winter most of the above-canopy *H* was due to heat transfer between the forest canopy and atmosphere, not the atmosphere and snow-covered ground (Burns et al., 2013). Related to LE, there are two interesting observations in Fig. 2a. First, outside the growing season, daytime LE was larger than nighttime LE. This is presumably because air temperature is higher during the daytime which increases the saturation vapor pressure and results in a larger sublimation/evaporation rate (e.g., Dalton, 1802). Second, nighttime LE in winter was around $25\,W\,m^{-2}$ which decreased to $10\,W\,m^{-2}$ in summer. Despite warmer summer temperatures, we suspect the larger nocturnal LE in winter was due to the ubiquitous presence of a snowpack that serves as a source of sublimation/evaporation for 24 h every day (compared to summer when the ground periodically dries out). Also, winds are much stronger in winter which would promote higher evaporation. In the spring and summer LE increased during the day from around 50 to $150\,W\,m^{-2}$ due to increased forest transpiration. In July–August, as the soil dried out and warmed up, soil microbial activity increased (e.g., Scott-Denton et al., 2006),

BGD
12, 8939–9004, 2015

and NEE moved closer to having photosynthetic uptake of CO_2 balanced by respiration.

When winds are light and mechanical turbulence is small, decoupling between the air near the ground and above-canopy air can occur (e.g., Baldocchi et al., 2000; Baldocchi, 2003). The nocturnal NEE data shown in Fig. 2a have been calculated using the friction velocity (u_*) filtering technique (Goulden et al., 1996) which replaces NEE during periods of weak ground-atmosphere coupling ($u_* < 0.2\,\mathrm{m\,s^{-1}}$) with an empirical relationship between NEE and soil temperature. This leads to the question of whether the application of the filtering by u_* created the apparent increase in nocturnal NEE (or respiration) during the summer months. In Supplement Fig. S1, we include both the non-u_* filtered NEE along with ecosystem respiration calculated from the algorithm of Reichstein et al. (2005) and Lasslop et al. (2010). Though the u_* filter enhanced the value of ecosystem respiration by around $0.5\,\mu\mathrm{mol\,m^{-2}\,s^{-1}}$ compared to unfiltered NEE, the mid-summer increase was present in both. Ecosystem respiration calculated from the algorithm of Lasslop et al. (2010) was slightly larger than that from Reichstein et al. (2005) which was closer to the measured nocturnal values. Recent research in the ecosystem-flux community has suggested that the standard deviation of the vertical wind σ_w (e.g., Acevedo et al., 2009; Oliveira et al., 2013; Alekseychik et al., 2013; Thomas et al., 2013) or the Monin–Obukhov stability parameter (e.g., Novick et al., 2004) are better measures of decoupling than u_*; however, the results we show are not going to be strongly affected by which variable is used to determine the coupling state.

The daytime interannual variability of NEE, LE and H was larger than the nighttime interannual variability (Fig. 2b) due to the wide range of daytime surface solar conditions (e.g., clear or cloudy days). The peak in the interannual variability of daytime NEE during April and May was due to year-to-year differences in the timing of snowmelt and initiation of photosynthetic forest uptake of CO_2 at the site (Monson et al., 2005; Hu et al., 2010a). Though NEE interannual variability peaked at this time, there was no corresponding peak in LE or H variability.

BGD
12, 8939–9004, 2015

The average start of the warm season occurred when daytime NEE uptake was strong (greater than 8 µmol m^{-2} s^{-1}) and immediately followed the peak in NEE inter-annual variability (Fig. 2b). There was not a similar increase in NEE variability to mark the end of the warm season; however, the date when daytime NEE decreased sharply was the end of September. For this reason, we chose the end of September as the end of the warm-season. By choosing the end of September we also avoid periods in October when snowfall occurs. On average, the period we chose for the warm season started on 1 June and ended on 30 September as indicated by the vertical lines in Fig. 2.

Based on eight years of precipitation data from a nearby U.S. Climate Reference Network (USCRN) site, April had the most precipitation (with a mean of around 120 mm, most all of it falling as snow) followed by July with 90 mm of precipitation (Fig. S2a). April and July were also the months with the largest variability between years and the variations between years were about 50 % of the mean value (Fig. S2b). These trends generally agree with the long-term precipitation measurements from the LTER C-1 (1953–2012) station where the effect of undercatch by the LTER gauge is noticeable during the winter months. Further discussion on the precipitation measurements used in our study are in Appendix A1.

3.2 The effect of wet conditions on the diel cycle

After each day was organized into the precipitation categories described in Sect. 2.3, we observed a peak in precipitation during the early afternoon on wet days as would be expected for a mountain-plain type weather system (Fig. 3b1). Over the 14 years of our study, the average length of time for a dry period was around 2.5 days with a standard deviation of 3 days. Two days in a row with above-average rain (i.e., Wet2 days) was recorded around 90 times out of 1740 total warm-season days between 1999 and 2012 (Table 2). These rare events were typically the result of large-scale synoptic weather systems which explains why significant morning precipitation occurred on Wet2 days (i.e., Fig. 3b1).

BGD
12, 8939–9004, 2015

One obvious complication with the precipitation-related analysis is that the open-path instrumentation (e.g., sonic anemometers) are affected by water droplets, and do not work properly during heavy precipitation events which is why the percent of gap-filling periods for the fluxes increases on the wet days (Table 2). Though we do not have a way around this issue, we can only point out that the scalar measurements were not affected by precipitation and can provide some degree of insight. When we restricted the analysis to time periods without any gap-filled flux data, the results are similar to what we are showing here.

Over the next several sections we will examine how the diel cycle of the measurements (winds, soil properties, radiation, scalars, and fluxes) were affected by these different precipitation states. Because Dry1 conditions were the most common, we will typically describe the changes or differences relative to the Dry1 state.

3.2.1 Wind, turbulence, and near-ground stability

As mentioned in Sect. 2.1, the above-canopy wind direction at the site is primarily controlled by the large-scale mountain-plain dynamics resulting in directions that were typically either upslope (from the east) or downslope (from the west). At night, the above-canopy winds were almost exclusively downslope with very little effect from precipitation except for a small occurrence of upslope flow during Wet2 conditions (i.e., Fig. 3a1). There was a more consistent flow direction in the early morning hours as demonstrated by the higher peak in the frequency distribution of Fig. 3a1 compared to Fig. 3a3. This suggests that the drainage flow became more persistent and consistent as the night progresses. During mid-day, wet conditions had a more frequent occurrence of upslope winds than downslope winds, whereas during dry days there was nearly an equal number of upslope and downslope winds (Fig. 3a2). This is to be expected because the upslope winds can trigger convection which (potentially) leads to precipitation.

The diel cycle of horizontal wind speed during dry conditions was characterized by a dip of about $1\,m\,s^{-1}$ during the morning and evening transitions, with the evening

BGD
12, 8939–9004, 2015

transition having the lowest wind speed values (Fig. 3c1). On Dry1 and Dry2 days the wind speed overnight (on average) increased from a minimum of around 2.5 $m s^{-1}$ at 19:00 MST to a maximum of 4 $m s^{-1}$ at 04:00 MST. During wet conditions the dip in wind speed during the transition periods did not exist and the mean wind speed on Wet2 days was typically smaller than other conditions throughout the diel cycle. Mechanical turbulence (characterized by the friction velocity u_*) generally follows the pattern of wind speed at night, however, during the daytime, the buoyancy generated by surface heating enhanced u_* relative to nocturnal values (Fig. 3d1). In Dry1 conditions the maximum variability in U and u_* was in the early morning (at around 06:00 MST) with less variability in the late afternoon and evening.

Near-ground vertical air temperature differences are considered because these help control the near-ground stability (Fig. 4d–f). In Wet2 conditions, the vertical air temperature difference was at a minimum during all times of the day. This is expected during the daytime because solar radiation, which warms the canopy and ground to create the air-surface temperature differences, was reduced on Wet2 days (radiation will be discussed in Sect. 3.2.3). In Dry2 conditions during daytime, the mid-canopy was about 1 °C warmer than the air near the ground (Fig. 4e). This stable layer in the lower canopy did not exist in any other conditions and we presume this state was due to a combination of strong net radiation (which warmed the canopy) combined with evaporation near the ground (which cooled the ground surface). The soil during a Dry2 day would have recently experienced rain, providing a source of liquid water for evaporation within the soil. We also note that temperature differences during Dry1 days were the largest of all precipitation states for the three periods shown in Fig. 4d–f.

To combine the effects of wind speed and temperature differences on atmospheric stability, the bulk Richardson number Ri_b is also considered (Fig. 3e1). Following the evening transition, dry conditions tended to result in a more stable atmosphere ($Ri_b > 0.2$) than that of wet conditions ($Ri_b < 0.1$). This suggests that there should be larger vertical scalar differences (i.e., less vertical mixing) during the late evening period of dry days.

BGD
12, 8939–9004, 2015

3.2.2 Atmospheric scalars (T_a, q, CO_2), soil temperature, soil moisture, and soil heat flux

We now consider how air temperature and other scalars change over the diel cycle. Dry1 conditions were associated with slightly higher barometric pressure (Fig. 5a1), relatively warmer air temperatures (Fig. 5b1), a drier atmosphere (Fig. 5c1), warmer and drier soils (Fig. 5d1 and e1), and larger soil heat fluxes (Fig. 5f1). Barometric pressure had a mid-morning and evening peak that existed for all precipitation states which are created by thermal tides within the atmosphere (e.g., Lindzen and Chapman, 1969). The variables for Dry1 days generally had smaller variability compared to any of the other conditions (Fig. 5a2–f2) with the one exception being a high variability in VPD during the Dry1 afternoon and evening period (Fig. 5c2). In contrast to Dry1 days, mean conditions during Wet2 days were associated with (relatively) lower barometric pressure and cooler, wetter conditions in the atmosphere and soil.

For Wet2 days, the soil moisture content (VWC) increased by over 50 % and T_{soil} dropped by around 2 °C relative to Dry1 conditions (Table 3 and Fig. 5d1 and e1). The timing of precipitation within the diel cycle is important. For example, on the morning of Wet1 days, T_{soil} was about 1 °C larger than in other conditions because on Wet1 days the rain occurred primarily in the afternoon, not the morning (i.e., Fig. 3b1). In fact, 21.5 m air temperature on the morning of Wet1 days was slightly above that of Dry1 days (Fig. 5b1). The main effect of precipitation on the soil heat flux was between the hours of 11:00 and 18:00 MST, where G in Dry1 conditions had a peak of 20 W m^{-2} while in Wet2 conditions the peak was less than 10 W m^{-2} (Fig. 5f1). At night, G was similar for all precipitation states suggesting that either the soil was protected from the effect of changes in nocturnal net radiation by the overlying canopy or else the changes in R_{net} were small enough that the soil temperature was not dramatically affected. This result also implies that increased liquid water in the soil pore space did not significantly affect the soil thermal conductivity. Though the soil heat flux peaked at around mid-day the soil temperature peaked two hours later at around 14:00 MST.

BGD
12, 8939–9004, 2015

If plots for each precipitation condition are arranged in the order of Dry1, Wet1, Wet2, and Dry2 days the characteristics of a composite summertime cold-front passing the tower can be approximated (Fig. 6). Classical cold-front systems over flat terrain are associated with pre-frontal wind shifts and pressure troughs (e.g., Schultz, 2005). Mountains, however, have a large impact on the movement of air masses and can considerably alter the classical description of frontal passages (e.g., Egger and Hoinka, 1992; Whiteman, 2000). Our classification of the composite plots as a "frontal passage" is simply because there was colder air present at the site during the Wet1 and Wet2 periods. For example, during Dry1 days the 21.5 m air temperature was around 5 °C greater than T_{soil} (Fig. 6b1). As the composite "front" passed by the tower (i.e., Wet1 and Wet2 days) 21.5 m T_a dropped to near T_{soil} (Fig. 6b2 and b3) and specific humidity increased by ≈ 50 % (Fig. 6c2 and c3). After the frontal passage (i.e., Dry2 days), the 21.5 m air temperature returned to being higher than the soil temperature (Fig. 6b4). During Wet2 days, CO_2 dry mole fraction χ_c within the canopy was elevated relative to the other conditions (Fig. 6d3). Specific numerical values and a summary of the atmospheric conditions for each precipitation state are provided in Table 3.

Taking a closer look at CO_2, we found that above-canopy χ_c was largest during Wet2 conditions and lowest in Dry1 conditions with a fairly consistent difference of around 2–3 µmol mol^{-1} across the entire diel cycle (Fig. 7a). We initially considered this to be an artifact of dilution due to boundary layer height differences (e.g., Culf et al., 1997), however we ruled this out because the difference was fairly consistent throughout the day and night when boundary layer heights change dramatically. We confirmed that similar differences between precipitation states existed using CO_2 from a nearby Rocky Raccoon site above tree-line on Niwot Ridge (Stephens et al., 2011) (results not shown). Since our analysis uses a composite which approximates a cold-front passage, there is an influence of large-scale weather systems on the overall atmospheric CO_2 magnitude (e.g., Miles et al., 2012; Lee et al., 2012). This suggests that the dependence of above-canopy χ_c on the precipitation state was due to either the composition of large-scale air masses or subsidence/convergence caused by high/low barometric pressure.

BGD
12, 8939–9004, 2015

Within the canopy, this same precipitation-dependent pattern existed in the morning and during the daytime, however, in the evening, χ_c in dry conditions was about 5–8 µmol mol^{-1} larger than χ_c in wet conditions (Fig. 7b–c). These differences clearly show up in a vertical χ_c profile (Fig. 8c). To avoid the confounding factor of synoptic weather systems, the lower panels in Fig. 8 show the vertical χ_c differences ($\Delta\chi_c$) relative to the top tower level (21.5 m a.g.l.). The mid-day $\Delta\chi_c$ profile (Fig. 8e) shows a photosynthetic deficit of around 1 µmol mol^{-1} in the mid-canopy due to vegetative uptake of CO_2 which is consistent with previous studies at the site (Bowling et al., 2009; Burns et al., 2011). In the nighttime hours (00:00–04:00 MST) the different precipitation states did not affect the $\Delta\chi_c$ profile (Fig. 8d) which contrasts with the late evening $\Delta\chi_c$ profile that shows a difference of around 5–9 µmol mol^{-1} between wet and dry conditions within the lower canopy (Fig. 8f).

Synoptic barometric pressure changes have recently been suggested as a mechanism for enhancing the exchange of deep-soil CO_2 with the atmosphere, whereas the upper soil CO_2 is more influenced by processes such as soil respiration and pressure-pumping (e.g., Sánchez-Cañete et al., 2013). In light of the differences in near-ground stability during the evening (discussed in Sect. 3.2.1), it seems likely that atmospheric stability was playing a more important role than barometric pressure in controlling the observed nocturnal $\Delta\chi_c$ differences. A close examination of Fig. 8f reveals that the late evening wet conditions had near-ground to above-canopy $\Delta\chi_c$ differences that were around 35 µmol mol^{-1}. In contrast, for all conditions in Fig. 8d and dry conditions in Fig. 8f the $\Delta\chi_c$ differences were greater than 40 µmol mol^{-1} (also see Table 3). The larger $\Delta\chi_c$ differences in dry conditions are consistent with the near-ground atmospheric stability being larger during dry conditions. We also note that between 00:00–04:00 MST Ri_b was generally near or above 0.2 for both wet and dry conditions while in the evening period the wet days had $Ri_b \approx 0.1$. As shown in previous work at the US-NR1 site (e.g., Schaeffer et al., 2008a; Burns et al., 2011), $\Delta\chi_c$ differences have a transition region between weakly stable and strongly stable conditions that occurs at $Ri_b \approx 0.25$ which is nominally related to the change from a fully turbulent to non-

BGD
12, 8939–9004, 2015

turbulent flow. It appears that the stability in the early evening on wet days is such that the atmosphere was slightly unstable which enhanced the vertical mixing and reduced the vertical $\Delta\chi_c$ differences. Furthermore, the controls on the stability between Wet1 and Wet2 days were slightly different. On Wet1 evenings, wind speed was slightly elevated (Fig. 3d1) which resulted in less stable conditions. In contrast, on Wet2 evenings it was the reduced vertical temperature differences (Fig. 4f) that was the primary controlling factor in reducing the stability.

3.2.3 Net radiation, turbulent energy fluxes, and net ecosystem exchange of CO_2 (NEE)

The full diel cycle of net radiation, the turbulent energy fluxes, and NEE are shown in Fig. 9 for mean values (a1–d1) and variability or SD-Bin (a2–d2). In order to better quantify the impact of precipitation on the fluxes, we have arranged the fluxes by Dry1, Wet1, Wet2, and Dry2 conditions similar to what was shown previously with the scalar measurements (i.e., Fig. 6). This summary, however, only includes mean mid-day (Fig. 10, left-column) and late evening and nighttime values (Fig. 10, right-column). Choosing these specific periods avoids the evening and morning transition periods which are complicated by the fluxes and scalar gradients becoming small and/or changing sign (e.g., Lothon et al., 2014). To make interpretation of the quantitative changes more accessible, each panel in Fig. 10 shows the fractional change from the maximum (or minimum) value within that panel. In addition to the figures, the mean values for each precipitation state are listed in Table 3.

When precipitation occurred, cloudiness increased and net radiation at mid-day was reduced (Fig. 9a1). Dry1 days had a mean mid-day value of nearly 600 $W m^{-2}$ which decreased by around 50 % to 300 $W m^{-2}$ during Wet2 days, then recovered on Dry2 days to nearly 550 $W m^{-2}$ (i.e., about 10 % smaller than R_{net} during Dry1 conditions) (Fig. 10a1). The variability of R_{net} was similar for all precipitation conditions, though Dry1 conditions typically had the smallest variability during the morning hours (Fig. 9a2).

BGD
12, 8939–9004, 2015

At night, though the absolute value of the mean net radiation was an order of magnitude smaller than the daytime values, the fractional changes and pattern of nocturnal R_{net} due to different precipitation states (Fig. 10a2) were similar to those of mid-day R_{net} (Fig. 10a1). If we assume that wet nights were cloudier than dry nights, the radiative surface cooling on clear nights was around $-70\,W\,m^{-2}$ while cloudy nights was closer to $-30\,W\,m^{-2}$. The reduction of the magnitude of R_{net} on wet nights was primarily due to changes in cloud cover as well as changes to the turbulent fluxes.

Sensible heat flux during mid-day had a similar pattern to net radiation, with a large decrease in H (by $\approx 70\,\%$) between Dry1 and Wet2 conditions, followed by an increase toward Dry1 H on Dry2 days (Fig. 10d1). In contrast, latent heat flux followed a slightly different pattern – the largest mean mid-day LE occurred on a Dry2 day with a value of around $200\,W\,m^{-2}$, which was around 15 % larger than mid-day LE on Dry1 days (Fig. 10c1). The extra energy used by LE (coupled with slightly lower R_{net} values on Dry2 days) explains why mid-day H only recovered to within $80\,W\,m^{-2}$ (or 30 %) of Dry1 H (Fig. 9d1) as dictated by the SEB equation (1).

The increased LE values on Dry2 days was presumably due to evaporation of the intercepted liquid water present on vegetation and in the soil. Because of the effect of temperature on saturation vapor pressure (and thus VPD) one cannot assume that nocturnal LE is representative of daytime evaporation (e.g., Brutsaert, 1982). To further explore this issue, we have plotted LE vs. VPD in Fig. 11 where we observe that nocturnal LE in dry conditions was $\approx 10\,W\,m^{-2}$ with a weak dependence on VPD. This is consistent with our assumption that there was a small, consistent baseline level of evaporation in dry conditions. Therefore, in Dry1 conditions we can estimate that evaporation was $\approx 10\,W\,m^{-2}$ and evapotranspiration was $\approx 170\,W\,m^{-2}$ (based on mid-day LE, Fig. 10c1). This suggests that, on average, evaporation comprised about 6 % of evapotranspiration in dry conditions. Since net radiation in Dry1 and Dry2 conditions was similar, we can get a rough estimate of daytime evaporation from the LE difference during Dry1 and Dry2 conditions (shown as a black line in Fig. 11a2). As the atmosphere becomes drier the LE difference increased from near $15\,W\,m^{-2}$ to around

BGD
12, 8939–9004, 2015

50 W m^{-2} where it flattens out in drier conditions (for VPD > 1.2). Previous research at the US-NR1 site has shown large differences in transpiration between the dominant tree species (Hu et al., 2010b), but the general relationship between ecosystem-scale transpiration and VPD is similar to what is shown in Fig. 11a2 (Turnipseed et al., 2009). Therefore, following a rain event, daytime evaporation was somewhere between 15–50 W m^{-2} (black line in Fig. 11a2) while mid-day evapotranspiration increased from 100–225 W m^{-2} (Dry2 line in Fig. 11a2). If we take the overall average of this ratio, it suggests that evaporation comprised about 20 % of evapotranspiration in wet conditions.

We also observed that increased LE lasted throughout a Dry2 day until around 18:00 MST when LE came within around 10 % of LE in Dry1 conditions (Figs. 9c1 and 11a3). This suggests that the evaporative effect lasted at least 18 h following a significant precipitation event. Central to our calculations is the assumption that LE at night was primarily evaporation. Some evidence exists that the needle stomates opening at night combined with cuticular water loss could lead to small amounts of nocturnal transpiration (e.g., Novick et al., 2009). If this occurred at US-NR1, it is likely a small effect which is further discussed by Turnipseed et al. (2009). We should also emphasize that our results are mean estimates and the variability around these mean values are large (i.e., as shown in Fig. 11b1–b4). Some of this variability is due to the random nature of turbulence in the atmosphere, whereas some can be explained by differences in net radiation, atmospheric stability, air temperature, and stomatal control.

The modeling study of Moore et al. (2008) based on sap flow measurements at the US-NR1 site found that transpiration in the warm-season accounted for about 30 % of total evapotranspiration, whereas our findings suggest that transpiration accounted for between 80 % (wet conditions) to 94 % (dry conditions) of evapotranspiration. The large discrepancy between these estimates and the model results might be due to the simplicity of the model used by Moore et al. (D. J. P. Moore, personal communication, 2015). Compared to eddy-covariance techniques, sap flow sensors have typically underestimated transpiration and there are scaling issues to contend with as well as other

BGD
12, 8939–9004, 2015

measurement challenges (e.g., Hogg et al., 1997; Wilson et al., 2001; Staudt et al., 2011). The trend toward less evaporation in Dry1 conditions is consistent with a large resistance to evaporation being present when the soil/litter surface under a canopy is dry (Baldocchi and Meyers, 1991). Based on lysimeter measurements of evaporation, it was found that transpiration comprised about 95 % of total evapotranspiration during the growing season in a boreal aspen forest (Blanken et al., 2001). The partitioning of evapotranspiration for a forest is strongly dependent on the vegetation density and modeling efforts by Lawrence et al. (2007) suggest that, for a canopy density similar to that of the US-NR1 forest (i.e., LAI ≈ 4), transpiration should be around 80 % of evapotranspiration. The spruce forest studied by Staudt et al. (2011) with LAI ≈ 4.8 found that transpiration accounted for about 90 % of total evapotranspiration (in generally dry conditions).

On a larger (global) scale it has recently been suggested from isotope measurements that transpiration contributes 80–90 % to the total annual terrestrial evapotranspiration (Jasechko et al., 2013). This result appears consistent with our estimate of transpiration for the warm-season months; however, similar to the GLEES Rocky Mountain forest site described by Schlaepfer et al. (2014), the US-NR1 forest only has active transpiration for 4–5 months of the year (e.g., Fig. 2a) so the annual contribution of transpiration is much reduced and sublimation of snow plays a significant role.

At night, latent heat flux cooled the surface and was strongly affected by changes in the precipitation state (Fig. 10c2) following a pattern similar to that of nocturnal R_{net} (Fig. 10a2). Nocturnal sensible heat flux changed by around 30–40 % during the different precipitation states but the pattern did not clearly follow that of either R_{net} or LE (Fig. 10d2). At night, H generally warms the surface (including the forest vegetation and other biomass) following the air-surface temperature gradient (i.e., similar to the vertical temperature differences shown in Fig. 4d and f). In this way, H acts to compensate for air-surface temperature differences that might be generated by the surface cooling effects of R_{net} and LE. Even though the vertical air temperature differences were largest during Dry1 conditions (Fig. 4d and f) the largest sensible heat flux occurred

BGD
12, 8939–9004, 2015

during Dry2 periods between 00:00–04:00 MST (Fig. 10d2). This is exactly when LE was at a maximum (so evaporative cooling would be expected) and a close look at Fig. 4f reveals that the temperature difference between the air just above the ground and soil was larger in Dry2 conditions than Dry1 conditions. We should also note that what is shown in Fig. 4d and f are vertical air temperature differences which serve as a surrogate for the actual difference between air temperature and the surface elements (i.e., tree branches, needles, boles, and the soil surface) (e.g., Froelich et al., 2011).

As one would expect, daytime NEE was reduced during wet conditions due to decreased photosynthetically active radiation (PAR) which is shown as a decrease in R_{net} in Fig. 9a1. The ratio between mid-day PAR and R_{net} was similar for all precipitation states (Table 3) and we will use R_{net} as a surrogate for PAR in our discussion. The Dry2 days were when the forest was most effective at assimilating CO_2 and NEE increased by over 3 $\mu mol\, m^{-2}\, s^{-1}$ ($\approx 30\,\%$) between Wet2 and Dry2 days (Fig. 10b1).

Nocturnal NEE was not affected very much (less than 10 %) by changes in the precipitation state and any effect was overshadowed by the difference between NEE in the late evening compared to the early morning (Figs. 9b1 and 10b2). The models of respiration by Reichstein and Lasslop produced results similar to the measured nocturnal NEE. The good agreement between the 14 year smoothed nighttime NEE measurement and R_{eco} calculated from the flux-partitioning (i.e., Fig. S1nocturnal ecosystem respiration signal was, at least for the seasonal-scale, captured at the 21.5 m measurement level.

The striking difference between the effect of precipitation on the transport of CO_2 (NEE) compared to water vapor (LE) is perplexing because one would expect the turbulence to transport water vapor and CO_2 in a similar manner. A few possible reasons for this difference are: (1) soil respiration at the US-NR1 site was not strongly affected by precipitation, (2) long dry periods are rare enough that the Birch effect (i.e., CO_2 pulse following precipitation) did not have a large impact on the overall warm-season NEE statistics, (3) the measurement of NEE at 21.5 m was not accurately describing the soil respiration at the soil surface due to surface decoupling and/or other prob-

BGD
12, 8939–9004, 2015

lems related to stable conditions (e.g., Staebler and Fitzjarrald, 2004; Finnigan, 2008; Aubinet, 2008; Thomas et al., 2013; Alekseychik et al., 2013), or (4) the difference in vertical location of these two scalar sources (e.g., liquid water evaporates from the vegetation surfaces as well as at the ground whereas respiration of CO_2 occurs almost exclusively at the ground) caused differences in the sensitivity to precipitation (Edburg et al., 2012). Previous measurements (mostly during the daytime) of soil respiration R_{soil} at US-NR1 with a manual chamber system by Scott-Denton et al. (2003, 2006) found that the dependence of soil respiration on soil moisture over a given summer was small. It has also been suggested by Huxman et al. (2004, 2003) that ecosystem respiration at the US-NR1 site is subject to controls from temperature and radiation as much as from precipitation (in contrast to an arid or semi-arid ecosystem such as a desert grassland where R_{eco} is strongly dependent on precipitation). The CO_2 pulse related to the Birch effect has been detected by eddy-covariance at a wide variety of ecosystems that are listed in the introduction. For the current study, the relevant results are: (i) the 21.5 m nocturnal NEE measurements were able to detect the increase in nocturnal ecosystem respiration over the warm-season (Fig. 2a), and (ii) the nocturnal NEE was not strongly affected by precipitation (Fig. 10b2). This suggests that, at the seasonal/annual time-scale, precipitation plays a minor role in modifying the contribution of ecosystem respiration to the above-canopy NEE for this subalpine ecosystem.

So far we have primarily discussed the mean changes to the ecosystem fluxes due to precipitation. Since these flux calculations are affected by turbulent atmospheric motions that have a large random component (e.g., Baldocchi, 2003; Vickers et al., 2009) and there is natural day-to-day (and seasonal) variability during a particular time of day, the variability (SD-Bin) around the mean flux value is large (Fig. 9a2–d2). Typically, SD-Bin for the flux is on the order of 50 % of the mean flux. The variability also provides some insight into the various physical processes taking place. For example, Dry1 conditions resulted in the smallest variability for mid-day NEE and LE, but not for H. Furthermore, in the morning hours (07:00–10:00 MST), the variability of both NEE and LE was largest for Wet2 conditions (Fig. 9b2–c2). This shows the connec-

BGD
12, 8939–9004, 2015

tion that NEE and LE have through the opening of stomates that provide pathways for both transpiration and photosynthesis. The fact that the variability for LE was elevated during Dry2 conditions (both between 00:00–04:00 MST and throughout the day) was due to the extra evaporation that occurs in Dry2 conditions as discussed above. These changes to LE also increased the Dry2 variability of sensible heat flux between 00:00–04:00 MST, but not in the evening hours. For models of ecosystem processes, the mean is often emphasized, but we point out that it is also important to understand the day-to-day variability in diel composites.

3.3 Asymmetry in the diel cycle of net radiation and turbulent fluxes

One other interesting aspect of the diel cycle is related to the timing of fluxes relative to solar noon. As one would expect, the top of the atmosphere radiation reached a maximum near 12:00 MST (Fig. 9a1). In contrast, the maximums for composited R_{net}, LE, and H occurred at about 11:00 MST on dry days and 10:00 MST on wet days (Fig. 9a1, c1–d1). For NEE, the peak uptake of CO_2 was between 09:00–10:00 MST on both wet and dry days (Fig. 9b1). The fact that the peak in the energy fluxes was different for wet and dry conditions suggests that clouds were affecting the composited diel cycle.

In Fig. 12 we further examine the role of clouds on the diel cycle by sub-dividing the Dry1 days into clear sky (Dry1-Clear) and cloudy (Dry1-Cloudy) days. Clear skies occurred on about 18 % of the Dry1 days and this is reflected by the fact that the Dry1 statistics closely follow those of Dry1-Cloudy statistics. The peak in R_{net}, LE, and H during Dry1-Clear days were all near 12:00 MST which was consistent with the timing of the maximum top of the atmosphere radiation.

On Dry1-Clear days, R_{net} was enhanced by an additional 30 % compared to cloudy days (Fig. 12a1). This enhanced incoming radiation was reflected by larger turbulent energy (LE and H) fluxes on Dry1-Clear days (Fig. 12c1–d1). Consistent with the findings by Monson et al. (2002), NEE was slightly smaller on days with clear skies suggesting that the forest was taking up more CO_2 when clouds were present (Fig. 12b1). This result is partially due to CO_2 uptake by vegetation reaching a saturation point

BGD
12, 8939–9004, 2015

with increasing radiation (e.g., Ruimy et al., 1995), as well as research that has shown diffuse radiative conditions are more conducive to photosynthetic uptake of CO_2 by vegetation (e.g., Gu et al., 1999, 2002; Law et al., 2002; Wang et al., 2008). (Further discussion is in Monson et al., 2002). If LE was completely controlled by stomates, one would expect that LE would follow NEE and be larger on Dry1-Cloudy days. However, the effect of much higher R_{net} on clear days also affects LE (through the SEB equation) and drives it to slightly higher levels on Dry1-Clear days.

The variability of net radiation during Dry1-Clear days closely approximated the variability of the top of the atmosphere radiation (Fig. 12a2) which suggests we successfully selected the clear days. It is also of note that the variability of mid-day sensible heat flux (Fig. 12a2) was strongly affected by clouds (similar to R_{net}), whereas the variability of mid-day NEE and especially LE were only slightly changed by clouds. This is an example of the unique connections between R_{net} and H compared to those between NEE and LE.

3.4 The surface energy balance (SEB) closure

Though the individual components in the SEB balance equation (i.e., Eq. 1) were dramatically affected by precipitation (i.e., Fig. 10), the overall mean simple SEB closure fraction during mid-day was fairly consistent at around 0.7–0.8 (Fig. 13a1). The missing 20 % in the energy closure is similar to that observed by previous studies at the site (e.g., Turnipseed et al., 2002; Burns et al., 2012). This suggests that the turbulent fluxes were consistently measured for each precipitation state and whatever is causing the missing 20 % is likely unrelated to precipitation.

The nighttime simple surface energy balance closure during the evening hours (19:00–23:00 MST) was at around 40–50 % while closure during the early morning hours (00:00–04:00 MST) was closer to 60–70 %. Any effect of precipitation on the SEB at night was overshadowed by these large differences related to the time of day. The effect of drainage flows on horizontal CO_2 advection at US-NR1 have been summarized in previous studies (e.g., Sun et al., 2007; Yi et al., 2008) and our objective

BGD
12, 8939–9004, 2015

is to point out that the SEB was most affected in the late evening and improved after midnight, presumably because the wind speed and variability of mechanical turbulence increased. This result is consistent with the findings of Burns et al. (2011) that there is increased turbulence variability in the nocturnal boundary layer after around 23:00 MST. However, we have also reported (in Sect. 3.2.1) that stability tends to get stronger as the night progresses, especially in Dry1 conditions. Though outside the scope of the current study, our suspicion is that as the stability and wind speed increase during the night it leads to the formation of intermittent turbulent events caused by increased wind shear. In terms of precipitation, it is clear that the pattern of stability was disrupted by the rain event (affecting both the wind speed and vertical temperature gradients) and the dry periods tended to be more stable ($Ri_b > 0.2$) at night than the wet periods ($Ri_b < 0.2$) as shown in Fig. 13c2. The decreased stability in wet conditions is especially prevalent in the early evenings as discussed previously in relation to the vertical CO_2 profiles (Sect. 3.2.2). Changes in VPD were closely related to changes in air temperature as reflected in how mean VPD changed with the precipitation state (Fig. 13b1 and b2). It is interesting that the pattern for nocturnal VPD (Fig. 13b2) was similar to that of stability (Fig. 13c2).

4 Summary and conclusions

Based on fourteen years of 30 min measurements, the typical seasonal cycle and interannual variability of turbulent fluxes of sensible and latent heat and NEE from just-above a high-elevation subalpine forest were presented. We used the snowpack ablation date to determine the start of the warm-season and related this to the smoothed annual fluxes. The warm-season was further analyzed to determine how precipitation perturbed the ecosystem fluxes on a diel (i.e., hourly) time-scale. A simple, novel conditional sampling method based on whether the mean daily precipitation was greater than 3 mm day^{-1} was used which essentially created a 4 day composite of a cold front passing by the tower (the dry days prior to the cold front, a day when the precipitation

BGD
12, 8939–9004, 2015

started, a day with precipitation on the preceding day, and the day following the precipitation event). Though the wet days comprised only 17 % of the warm-season days, they accounted for around 85 % of the total precipitation.

The results showed what might be expected for a cold-front passage in a mountainous location: an afternoon peak in precipitation, a 6 °C drop in air temperature, and a 50 % increase in specific humidity. Changing from dry conditions to the wet, cool period of the composite front, we found the following changes during mid-day: net radiation decreased from around 585 to 275 $W m^{-2}$ (over 50 %), sensible heat flux decreased from 280 to 85 $W m^{-2}$ (around 70 %), latent heat flux was reduced from 170 to 125 $W m^{-2}$ (around 25 %), and NEE was reduced from −7.8 to −5.4 $\mu mol m^{-2} s^{-1}$ (around 30 %). Despite these dramatic changes to the individual component energy fluxes, the simple surface energy balance (SEB) closure during the daytime remained between 70–80 % throughout the 4 day composite frontal passage (Fig. 13a1). This level of SEB closure is consistent with previous studies at the site (e.g., Turnipseed et al., 2002; Burns et al., 2012) and suggests that whatever is causing the closure imbalance is a phenomena unrelated to precipitation and clouds.

For a typical day following a rain event, net radiation and sensible heat flux both recovered to slightly below dry-day values. Latent heat flux, however, increased from a dry-day value of 170 $W m^{-2}$ to nearly 200 $W m^{-2}$. Because LE also increased at night we conclude that LE increased due to evaporation of liquid water from the wet vegetation surfaces and ground. The enhanced LE due to evaporation lasted at least 18 h, after which time it returned to a value similar to that of dry conditions (Fig. 9c1). Another example of the effect of increased evaporation was the creation of a mid-day stable temperature layer within the forest sub-canopy (Fig. 4e). We conclude that the stable layer formed due to a combination of the vegetation being warmed by solar radiation and evaporative cooling near the ground. For NEE, we found that the subalpine forest at the US-NR1 site was most effective in assimilating CO_2 on the day following a significant rain event. A closer look at the diel cycle reveals that increased NEE occurred during the afternoon of a day following rain (Fig. 9b1).

BGD
12, 8939–9004, 2015

Any effect of precipitation on nocturnal NEE and SEB closure was overshadowed by the influence of low winds and drainage flows. Precipitation also disrupted the typical dry-day diel pattern in several distinct ways: (1) it eliminated the dip of $\approx 1\,m\,s^{-1}$ in above-canopy horizontal wind speed during the morning and evening transitions (Fig. 3c1), (2) it generally led to lower overall levels of mechanical turbulence (Fig. 3c2), and (3) it decreased the magnitude of subcanopy/above-canopy vertical air temperature differences (Fig. 4). These effects resulted in weakly stable conditions in the late evening during wet periods ($Ri_b \approx 0.1$) compared to the more strongly stable dry periods ($Ri_b \approx 0.2$). These stability differences contributed to smaller CO_2 vertical differences (relative to above-canopy CO_2) in the wet (less stable) conditions. After midnight, stability increased for both wet and dry conditions which created CO_2 vertical differences that were similar in both wet and dry conditions. Despite the stronger stability after midnight there was also increased wind speed and mechanical turbulence (especially in dry conditions) which should result in increased vertical mixing. Further examination of these nighttime phenomena are beyond the scope of the current study but are recommended for future investigations.

By comparing cloudy and cloud-free days during dry periods we found that clouds shifted the diel maximum in sensible and latent heat fluxes from 12:00 MST on clear days to around 11:00 MST on cloudy days. Also, mid-day net radiation and sensible heat flux were enhanced by about 20 % on clear days relative to cloudy days. In contrast, the timing of the peak in NEE (at around 10:00 MST) was unaffected by clouds and the forest was more efficient at assimilating CO_2 on cloudy days than clear days (Fig. 12b1).

Our study has provided an example of one way to look at the complex interconnections between variables that make modeling ecosystems so challenging. We have centered our study on precipitation, but these techniques could easily be adapted to focus on some over variable. Furthermore, this type of analysis could be used to evaluate models at the hourly time-scale (e.g., Matheny et al., 2014). We have shown that precipitation is intrinsically linked to changes in air temperature, pressure, and at-

BGD
12, 8939–9004, 2015

mospheric humidity. Our focus was on the local near-ground and source effects on the scalars and fluxes relative to precipitation. The atmospheric boundary layer, and specifically the boundary layer height and entrainment, will also have an impact on the near-surface scalar concentrations and fluxes (e.g., Culf et al., 1997; van Heerwaarden et al., 2009; Pino et al., 2012). Characteristics such as boundary-layer height are linked to the larger-scale flows at the mountainous US-NR1 research site and will be considered in a future study.

Appendix A: Additional data details

A1 Additional measurements

At US-NR1, the mean temperature and humidity profiles were measured with three mechanically aspirated, slow-response temperature-humidity sensors (Vaisala, model HMP35-D) installed at 2, 8, and 21.5 m a.g.l.. The vertical resolution of the temperature measurements was enhanced by a set of twelve unaspirated 0.254 mm diameter type-E chromel-constantan thermocouples distributed between the ground and 21.98 m a.g.l..

Precipitation was measured on the US-NR1 tower at 11.5 m (canopy top) with a tipping bucket rain gauge (Campbell Scientific, Met One Model 385) starting in late summer of 1999. Two nearby precipitation-measurement sites were used to check the Met One data quality and for gap-filling. One station was part of the U.S. Climate Reference Network (USCRN; Diamond et al., 2013) (site: CO Boulder 14 W, Mountain Research Station, Hills Mill) located about 700 m northeast of US-NR1. These measurements started in 2004 using a Geonor T-200B precipitation gauge with a Small Double Fence Intercomparison Reference (SDFIR) type of wind shield around the gauge. The second precipitation site was operated by the Niwot Ridge Long Term Ecological Research (LTER) Mountain Climate Program who used both a Geonor T-200B gauge (unshielded) and, for the longer-term record dating back to 1953, a Belfort precipita-

BGD
12, 8939–9004, 2015

tion gauge strip-chart recorder for daily precipitation amounts (e.g., Greenland, 1989; Williams et al., 1996). The LTER sensors were located about 550 m northeast of the US-NR1 tower. Though in winter the unshielded Met One gauge grossly underestimated total precipitation due to snow blowing by the tipping bucket gauge (e.g., Rasmussen et al., 2012), the warm-season cumulative precipitation between the USCRN and Met One gauges were typically within about 20 cm of each other (with a typical mean value of 250 cm). However, starting in summer of 2011, the Met One gauge started showing much greater precipitation amounts which we suspect was due to the "points" which hold the tipping bucket becoming worn and loose (in winter of 2013, the sensor failed completely). Therefore, the precipitation data used for the summers of 2011 and 2012 were exclusively from the USCRN sensor. Because the US-NR1 Met One sensor was not installed until late summer of 1999, the LTER Geonor data were used for the 1999 warm season. However, prior to year 2000, only daily precipitation was measured by LTER so hourly precipitation data were not available for 1999 which allows for the determination of a wet day, but not the diel cycle of precipitation.

Carbon dioxide dry mole fraction was measured on the US-NR1 tower with a tunable diode laser (TDL) absorption spectrometer (Campbell Scientific, model TGA100A) as described by Bowling et al. (2005); Schaeffer et al. (2008b). Measurements were made in summer of 2003 and continuously from fall of 2005 to the present. For our study, nine TDL inlets between 0.1 and 21.5 m a.g.l. were used to evaluate the CO_2 profile. The precision of TDL CO_2 mole fraction is estimated to be about 0.2 µmol mol^{-1} (Schaeffer et al., 2008b). For calculating the storage term in NEE, an independent CO_2-profile system with a closed-path IRGA (LI-COR, model LI-6251) was used as described in Monson et al. (2002). The TDL CO_2 data were downloaded on 7 January 2013 from http://biologylabs.utah.edu/bowling/.

A2 Updates to US-NR1 AmeriFlux data

The version of the US-NR1 AmeriFlux data used in our study (ver.2011.04.20) includes a correction for an error in the closed-path IRGA CO_2 flux calculation where a water-

BGD
12, 8939–9004, 2015

vapor correction was applied twice: first, as a sample-by-sample dilution correction and second by including the Webb–Pearman–Leuning (WPL) term in the CO_2 flux (e.g., Ibrom et al., 2007). After the error was discovered in Fall of 2010, the CO_2 flux (and NEE) for all years were re-calculated from the raw 10 Hz data with only the dilution correction applied and the updated/fixed data set was released on 20 April 2011 (http://urquell.colorado.edu/data_ameriflux/). Though the point-by-point difference between the correct and incorrect 30 min NEE values appears small, when accumulated over a year, the correctly-calculated NEE approximately doubled the annual uptake of CO_2 by the US-NR1 forest. The accumulation of a systematic measurement error over time is a well-known issue in the flux community (Moncrieff et al., 1996). Several side-by-side instrument comparisons by the AmeriFlux QA/QC team (e.g., Schmidt et al., 2012) have found the US-NR1 measurements to be of high quality (and also helped to assess the calculation error of the CO_2 flux).

The Supplement related to this article is available online at doi:10.5194/bgd-12-8939-2015-supplement.

Acknowledgements. We thank the Niwot Ridge LTER team (Katharine Suding, Mark Williams, Jennifer Morse, and many others) for maintaining the LTER instruments and making these data available. Dave Bowling, Don Lenschow, Arnold Moene, and Jielun Sun provided helpful discussions. We also appreciate site visits and evaluation of the US-NR1 measurements by the AmeriFlux QA/QC team (Sebastien Biraud, Stephen Chan, and Christoph Thomas). Carbon dioxide profile measurements were supported by grants to Dave Bowling from the U.S. Department of Energy (DOE), Office of Science, Office of Biological and Environmental Research, Terrestrial Ecosystem Science Program under Award Numbers DE-SC0005236 and DE-SC001625. We also acknowledge the U.S. Climate Reference Network (USCRN) for collecting high-quality data and creating a database that is accessible and simple. The US-NR1 AmeriFlux site is currently supported by the U.S. DOE, Office of Science through the AmeriFlux Management Project (AMP) at Lawrence Berkeley National Laboratory under Award Number 7094866. The National Center for Atmospheric Research (NCAR) is sponsored by NSF.

BGD
12, 8939–9004, 2015

References

Acevedo, O. C., Moraes, O. L. L., Degrazia, G. A., Fitzjarrald, D. R., Manzi, A. O., and Campos, J. G.: Is friction velocity the most appropriate scale for correcting nocturnal carbon dioxide fluxes?, Agr. Forest Meteorol., 149, 1–10, 2009. 8952

Alekseychik, P., Mammarella, I., Launiainen, S., Rannik, Ü., and Vesala, T.: Evolution of the nocturnal decoupled layer in a pine forest canopy, Agr. Forest Meteorol., 174–175, 15–27, 2013. 8952, 8964

Aubinet, M.: Eddy covariance CO_2 flux measurements in nocturnal conditions: an analysis of the problem, Ecol. Appl., 18, 1368–1378, 2008. 8964

Aubinet, M., Grelle, A., Ibrom, A., Rannik, U., Moncrieff, J., Foken, T., Kowalski, A. S., Martin, P. H., Berbigier, P., Bernhofer, C., Clement, R., Elbers, J., Granier, A., Grunwald, T., Morgenstern, K., Pilegaard, K., Rebmann, C., Snijders, W., Valentini, R., and Vesala, T.: Estimates of the annual net carbon and water exchange of forests: the EUROFLUX methodology, Adv. Ecol. Res., 30, 113–175, 2000. 8943

Aubinet, M., Berbigier, P., Bernhofer, C. H., Cescatti, A., Feigenwinter, C., Granier, A., Grunwald, T. H., Havrankova, K., Heinesch, B., Longdoz, B., Marcolla, B., Montagnani, L., and Sedlak, P.: Comparing CO_2 storage and advection conditions at night at different CARBOEUROFLUX sites, Bound.-Lay. Meteorol., 116, 63–94, 2005. 8949

Aubinet, M., Vesala, T., and Papale, D.: Eddy Covariance: A Practical Guide to Measurement and Data Analysis, Springer Atmospheric Sciences, Dordrecht, the Netherlands, 438 pp., 2012. 8947

Austin, A. T., Yahdjian, L., Stark, J. M., Belnap, J., Porporato, A., Norton, U., Ravetta, D. A., and Schaeffer, S. M.: Water pulses and biogeochemical cycles in arid and semiarid ecosystems, Oecologia, 141, 221–235, 2004. 8941

Baldocchi, D., Finnigan, J., Wilson, K., Paw, U. K. T., and Falge, E.: On measuring net ecosystem carbon exchange over tall vegetation on complex terrain, Bound.-Lay. Meteorol., 96, 257–291, 2000. 8952

Baldocchi, D. D.: Assessing the eddy covariance technique for evaluating carbon dioxide exchange rates of ecosystems: past, present and future, Glob. Change Biol., 9, 479–492, 2003. 8952, 8964

Baldocchi, D. D. and Meyers, T. P.: Trace gas-exchange above the floor of a deciduous forest. 1. Evaporation and CO_2 efflux, J. Geophys. Res., 96, 7271–7285, 1991. 8962

BGD
12, 8939–9004, 2015

Berkelhammer, M., Hu, J., Bailey, A., Noone, D. C., Still, C. J., Barnard, H., Gochis, D., Hsiao, G. S., Rahn, T., and Turnipseed, A.: The nocturnal water cycle in an open-canopy forest, J. Geophys. Res., 118, 1–18, 2013. 8943, 8948

Betts, A. K. and Ball, J. H.: The FIFE surface diurnal cycle climate, J. Geophys. Res., 100, 25679–25693, 1995. 8941

Blanken, P. D., Black, T. A., Yang, P. C., Neumann, H. H., Nesic, Z., Staebler, R., den Hartog, G., Novak, M. D., and Lee, X.: Energy balance and canopy conductance of a boreal aspen forest: partitioning overstory and understory components, J. Geophys. Res.-Atmos., 102, 28915–28927, 1997. 8943

Blanken, P. D., Black, T. A., Neumann, H. H., den Hartog, G., Yang, P. C., Nesic, Z., and Lee, X.: The seasonal water and energy exchange above and within a boreal aspen forest, J. Hydrol., 245, 118–136, 2001. 8943, 8962

Bonan, G.: Ecological Climatology: Concepts and Applications, Cambridge University Press, Cambridge, UK, 2nd edn., 550 pp., 2008. 8941

Borken, W. and Matzner, E.: Reappraisal of drying and wetting effects on C and N mineralization and fluxes in soils, Glob. Change Biol., 15, 808–824, 2009. 8942

Bowling, D. R., Burns, S. P., Conway, T. J., Monson, R. K., and White, J. W. C.: Extensive observations of CO_2 carbon isotope content in and above a high-elevation subalpine forest, Global Biogeochem. Cy., 19, GB3023, doi:10.1029/2004GB002394, 2005. 8971

Bowling, D. R., Miller, J. B., Rhodes, M. E., Burns, S. P., Monson, R. K., and Baer, D.: Soil, plant, and transport influences on methane in a subalpine forest under high ultraviolet irradiance, Biogeosciences, 6, 1311–1324, doi:10.5194/bg-6-1311-2009, 2009. 8958

Bowling, D. R., Grote, E. E., and Belnap, J.: Rain pulse response of soil CO_2 exchange by biological soil crusts and grasslands of the semiarid Colorado Plateau, United States, J. Geophys. Res., 116, G03028, doi:10.1029/2011JG001643, 2011. 8941

Bowling, D. R., Ballantyne, A. P., Miller, J. B., Burns, S. P., Conway, T. J., Menzer, O., Stephens, B. B., and Vaughn, B. H.: Ecological processes dominate the ^{13}C land disequilibrium in a Rocky Mountain subalpine forest, Global Biogeochem. Cy., 28, 352–370, doi:10.1002/2013GB004686, 2014. 8949

Brazel, A. J. and Brazel, S. W.: Summer diurnal wind patterns at 3000 m surface level, Front Range, Colorado, USA, Phys. Geogr., 4, 53–61, 1983. 8946

Brutsaert, W.: Evaporation into the Atmosphere, Kluwer Academic Publishers, Dordrecht, the Netherlands, 299 pp., 1982. 8943, 8960

BGD
12, 8939–9004, 2015

Burns, S. P., Sun, J., Lenschow, D. H., Oncley, S. P., Stephens, B. B., Yi, C., Anderson, D. E., Hu, J., and Monson, R. K.: Atmospheric stability effects on wind fields and scalar mixing within and just above a subalpine forest in sloping terrain, Bound.-Lay. Meteorol., 138, 231–262, doi:10.1007/s10546-010-9560-6, 2011. 8946, 8948, 8949, 8958, 8967

Burns, S. P., Horst, T. W., Jacobsen, L., Blanken, P. D., and Monson, R. K.: Using sonic anemometer temperature to measure sensible heat flux in strong winds, Atmos. Meas. Tech., 5, 2095–2111, doi:10.5194/amt-5-2095-2012, 2012. 8947, 8966, 8968

Burns, S. P., Molotch, N. P., Williams, M. W., Knowles, J. F., Seok, B., Monson, R. K., Turnipseed, A. A., and Blanken, P. D.: Snow temperature changes within a seasonal snowpack and their relationship to turbulent fluxes of sensible and latent heat, J. Hydrometeorol., 15, 117–142, doi:10.1175/JHM-D-13-026.1, 2013. 8945, 8947, 8951

Cuenca, R. H., Ek, M., and Mahrt, L.: Impact of soil water property parameterization on atmospheric boundary layer simulation, J. Geophys. Res., 101, 7269–7277, 1996. 8941

Culf, A. D., Fisch, G., Malhi, Y., and Nobre, C. A.: The influence of the atmospheric boundary layer on carbon dioxide concentrations over a tropical forest, Agr. Forest Meteorol., 85, 149–158, 1997. 8957, 8970

Dalton, J.: Experimental essays on the constitution of mixed gases; on the force of steam or vapour from water and other liquids at different temperatures, both in a Torricellian vacuum and in air; on evaporation and on the expansion of gas by heat, Mem. Manchester Lit. and Phil. Soc., 5, 535–602, 1802. 8951

Diamond, H. J., Karl, T. R., Palecki, M. A., Baker, C. B., Bell, J. E., Leeper, R. D., Easterling, D. R., Lawrimore, J. H., Meyers, T. P., Helfert, M. R., Goodge, G., and Thorne, P. W.: U.S. Climate Reference Network after one decade of operations: status and assessment, B. Am. Meteorol. Soc., 94, 485–498, 2013. 8970, 8988

Edburg, S. L., Stock, D., Lamb, B. K., and Patton, E. G.: The effect of the vertical source distribution on scalar statistics within and above a forest canopy, Bound.-Lay. Meteorol., 142, 365–382, 2012. 8964

Egger, J. and Hoinka, K. P.: Fronts and orography, Meteorol. Atmos. Phys., 48, 3–36, 1992. 8957

Finnigan, J.: An introduction to flux measurements in difficult conditions, Ecol. Appl., 18, 1340–1350, 2008. 8964

Froelich, N. J., Grimmond, C. S. B., and Schmid, H. P.: Nocturnal cooling below a forest canopy: model and evaluation, Agr. Forest Meteorol., 151, 957–968, 2011. 8963

BGD
12, 8939–9004, 2015

Garratt, J. R.: The Atmospheric Boundary Layer, Cambridge University Press, Cambridge, 316 pp., 1992. 8941
Goulden, M. L., Munger, J. W., Fan, S. M., Daube, B. C., and Wofsy, S. C.: Measurements of carbon sequestration by long-term eddy covariance: methods and a critical evaluation of accuracy, Glob. Change Biol., 2, 169–182, 1996. 8952
Greenland, D.: The climate of Niwot Ridge, Front Range, Colorado, USA, Arctic Alpine Res., 21, 380–391, 1989. 8971
Greenland, D.: Mountain climates, in: Encyclopedia of World Climatology, Encyclopedia of Earth Sciences Series, edited by: Oliver, J. E., Springer, Dordrecht, the Netherlands, 517–523, doi:10.1007/1-4020-3266-8_145, 2005. 8946
Grimmond, C. S. B., Isard, S. A., and Belding, M. J.: Development and evaluation of continuously weighing mini-lysimeters, Agr. Forest Meteorol., 62, 205–218, 1992. 8943
Gu, L. H., Fuentes, J. D., Shugart, H. H., Staebler, R. M., and Black, T. A.: Responses of net ecosystem exchanges of carbon dioxide to changes in cloudiness: results from two North American deciduous forests, J. Geophys. Res., 104, 31421–31434, 1999. 8966
Gu, L. H., Baldocchi, D., Verma, S. B., Black, T. A., Vesala, T., Falge, E. M., and Dowty, P. R.: Advantages of diffuse radiation for terrestrial ecosystem productivity, J. Geophys. Res., 107, 4050, doi:10.1029/2001JD001242, 2002. 8966
Hirano, T., Kim, H., and Tanaka, Y.: Long-term half-hourly measurement of soil CO_2 concentration and soil respiration in a temperate deciduous forest, J. Geophys. Res., 108, 4631, doi:10.1029/2003JD003766, 2003. 8941
Hogg, E. H., Black, T. A., den Hartog, G., Neumann, H. H., Zimmermann, R., Hurdle, P. A., Blanken, P. D., Nesic, Z., Yang, P. C., Staebler, R. M., McDonald, K. C., and Oren, R.: A comparison of sap flow and eddy fluxes of water vapor from a boreal deciduous forest, J. Geophys. Res., 102, 28929–28937, 1997. 8943, 8962
Hu, J., Moore, D. J. P., Burns, S. P., and Monson, R. K.: Longer growing seasons lead to less carbon sequestration by a subalpine forest, Glob. Change Biol., 16, 771–783, doi:10.1111/j.1365-2486.2009.01967.x, 2010a. 8943, 8945, 8950, 8952, 8992
Hu, J., Moore, D. J. P., Riveros-Iregui, D. A., Burns, S. P., and Monson, R. K.: Modeling whole-tree carbon assimilation rate using observed transpiration rates and needle sugar carbon isotope ratios, New Phytol., 185, 1000–1015, doi:10.1111/j.1469-8137.2009.03154.x, 2010b. 8961

BGD
12, 8939–9004, 2015

Huxman, T. E., Turnipseed, A. A., Sparks, J. P., Harley, P. C., and Monson, R. K.: Temperature as a control over ecosystem CO_2 fluxes in a high-elevation, subalpine forest, Oecologia, 134, 537–546, 2003. 8964

Huxman, T. E., Snyder, K. A., Tissue, D., Leffler, A. J., Ogle, K., Pockman, W. T., Sandquist, D. R., Potts, D. L., and Schwinning, S.: Precipitation pulses and carbon fluxes in semiarid and arid ecosystems, Oecologia, 141, 254–268, 2004. 8941, 8964

Ibrom, A., Dellwik, E., Larsen, S. E., and Pilegaard, K.: On the use of the Webb-Pearman-Leuning theory for closed-path eddy correlation measurements, Tellus B, 59, 937–946, 2007. 8972

Inglima, I., Alberti, G., Bertolini, T., Vaccari, F. P., Gioli, B., Miglietta, F., Cotrufo, M. F., and Peressotti, A.: Precipitation pulses enhance respiration of Mediterranean ecosystems: the balance between organic and inorganic components of increased soil CO_2 efflux, Glob. Change Biol., 15, 1289–1301, 2009. 8941

Irvine, J. and Law, B. E.: Contrasting soil respiration in young and old-growth ponderosa pine forests, Glob. Change Biol., 8, 1183–1194, 2002. 8941

Ivans, S., Hipps, L., Leffler, A. J., and Ivans, C. Y.: Response of water vapor and CO_2 fluxes in semiarid lands to seasonal and intermittent precipitation pulses, J. Hydrometeorol., 7, 995–1010, 2006. 8941

Jarvis, P., Rey, A., Petsikos, C., Wingate, L., Rayment, M., Pereira, J., Banza, J., David, J., Miglietta, F., Borghetti, M., Manca, G., and Valentini, R.: Drying and wetting of Mediterranean soils stimulates decomposition and carbon dioxide emission: the “Birch effect”, Tree Physiol., 27, 929–940, 2007. 8941, 8942

Jarvis, P. G. and McNaughton, K. G.: Stomatal control of transpiration: scaling up from leaf to region, Adv. Ecol. Res., 15, 1–49, 1986. 8943

Jasechko, S., Sharp, Z. D., Gibson, J. J., Birks, S. J., Yi, Y., and Fawcett, P. J.: Terrestrial water fluxes dominated by transpiration, Nature, 496, 347–351, 2013. 8943, 8962

Jenerette, G. D., Scott, R. L., and Huxman, T. E.: Whole ecosystem metabolic pulses following precipitation events, Funct. Ecol., 22, 924–930, 2008. 8941, 8942

Kaimal, J. C. and Finnigan, J. J.: Atmospheric Boundary Layer Flows: Their Structure and Measurement, Oxford University Press, New York, 289 pp., 1994. 8949

Katul, G. G., Oren, R., Manzoni, S., Higgins, C., and Parlange, M. B.: Evapotranspiration: a process driving mass transport and energy exchange in the soil-plant-atmosphere-climate system, Rev. Geophys., 50, RG3002, doi:10.1029/2011RG000366, 2012. 8943

BGD
12, 8939–9004, 2015

Kim, D., Oren, R., Oishi, A. C., Hsieh, C. I., Phillips, N., Novick, K. A., and Stoy, P. C.: Sensitivity of stand transpiration to wind velocity in a mixed broadleaved deciduous forest, Agr. Forest Meteorol., 187, 62–71, 2014. 8943

Knowles, J. F., Burns, S. P., Blanken, P. D., and Monson, R. K.: Fluxes of energy, water, and carbon dioxide from mountain ecosystems at Niwot Ridge, Colorado, Plant Ecol. and Diversity, doi:10.1080/17550874.2014.904950, 2014. 8945

Kollet, S. J., Cvijanovic, I., Schuttemeyer, D., Maxwell, R. M., Moene, A. F., and Bayer, P.: The influence of rain sensible heat and subsurface energy transport on the energy balance at the land surface, Vadose Zone J., 8, 846–857, 2009. 8941

Kottek, M., Grieser, J., Beck, C., Rudolf, B., and Rubel, F.: World map of the Köppen-Geiger climate classification updated, Meteorol. Z., 15, 259–263, doi:10.1127/0941-2948/2006/0130, 2006. 8946

Lasslop, G., Reichstein, M., Papale, D., Richardson, A. D., Arneth, A., Barr, A., Stoy, P., and Wohlfahrt, G.: Separation of net ecosystem exchange into assimilation and respiration using a light response curve approach: critical issues and global evaluation, Glob. Change Biol., 16, 187–208, 2010. 8949, 8952

Law, B. E., Williams, M., Anthoni, P. M., Baldocchi, D. D., and Unsworth, M. H.: Measuring and modelling seasonal variation of carbon dioxide and water vapour exchange of a Pinus ponderosa forest subject to soil water deficit, Glob. Change Biol., 6, 613–630, 2000. 8943

Law, B. E., Falge, E., Gu, L., Baldocchi, D. D., Bakwin, P., Berbigier, P., Davis, K., Dolman, A. J., Falk, M., Fuentes, J. D., Goldstein, A., Granier, A., Grelle, A., Hollinger, D., Janssens, I. A., Jarvis, P., Jensen, N. O., Katul, G., Mahli, Y., Matteucci, G., Meyers, T., Monson, R., Munger, W., Oechel, W., Olson, R., Pilegaard, K., Paw, K. T., Thorgeirsson, H., Valentini, R., Verma, S., Vesala, T., Wilson, K., and Wofsy, S.: Environmental controls over carbon dioxide and water vapor exchange of terrestrial vegetation, Agr. Forest Meteorol., 113, 97–120, 2002. 8943, 8966

Lawrence, D. M., Thornton, P. E., Oleson, K. W., and Bonan, G. B.: The partitioning of evapotranspiration into transpiration, soil evaporation, and canopy evaporation in a GCM: impacts on land-atmosphere interaction, J. Hydrometeorol., 8, 862–880, 2007. 8962

Lee, T. R., De Wekker, S. F. J., Andrews, A. E., Kofler, J., and Williams, J.: Carbon dioxide variability during cold front passages and fair weather days at a forested mountaintop site, Atmos. Environ., 46, 405–416, 2012. 8957

Lee, X., Wu, H. J., Sigler, J., Oishi, C., and Siccama, T.: Rapid and transient response of soil respiration to rain, Glob. Change Biol., 10, 1017–1026, 2004. 8941, 8942
Leuning, R., van Gorsel, E., Massman, W. J., and Isaac, P. R.: Reflections on the surface energy imbalance problem, Agr. Forest Meteorol., 156, 65–74, doi:10.1016/j.agrformet.2011.12.002, 2012. 8946
Lindzen, R. S. and Chapman, S.: Atmospheric tides, Space Sci. Rev., 10, 3–188, 1969. 8956
Lothon, M., Lohou, F., Pino, D., Couvreux, F., Pardyjak, E. R., Reuder, J., Vilà-Guerau de Arellano, J., Durand, P, Hartogensis, O., Legain, D., Augustin, P., Gioli, B., Lenschow, D. H., Faloona, I., Yagüe, C., Alexander, D. C., Angevine, W. M., Bargain, E, Barrié, J., Bazile, E., Bezombes, Y., Blay-Carreras, E., van de Boer, A., Boichard, J. L., Bourdon, A., Butet, A., Campistron, B., de Coster, O., Cuxart, J., Dabas, A., Darbieu, C., Deboudt, K., Delbarre, H., Derrien, S., Flament, P., Fourmentin, M., Garai, A., Gibert, F., Graf, A., Groebner, J., Guichard, F., Jiménez, M. A., Jonassen, M., van den Kroonenberg, A., Magliulo, V., Martin, S., Martinez, D., Mastrorillo, L., Moene, A. F., Molinos, F., Moulin, E., Pietersen, H. P., Piguet, B., Pique, E., Román-Cascón, C., Rufin-Soler, C., Saïd, F., Sastre-Marugán, M., Seity, Y., Steeneveld, G. J., Toscano, P., Traullé, O., Tzanos, D., Wacker, S., Wildmann, N., and Zaldei, A.: The BLLAST field experiment: Boundary-Layer Late Afternoon and Sunset Turbulence, Atmos. Chem. Phys., 14, 10931–10960, doi:10.5194/acp-14-10931-2014, 2014. 8959
Malhi, Y., Pegoraro, E., Nobre, A. D., Pereira, M. G. P., Grace, J., Culf, A. D., and Clement, R.: Energy and water dynamics of a central Amazonian rain forest, J. Geophys. Res.-Atmos., 107, 8061, doi:10.1029/2001JD000623, 2002. 8943
Marr, J. W.: Ecosystems on the east slope of the Front Range in Colorado, Series in Biology, No. 8, University of Colorado Press, Boulder, Colorado, 144 pp., 1961. 8945
Matheny, A. M., Bohrer, G., Stoy, P. C., Baker, I. T., Black, A. T., Desai, A. R., Dietze, M. C., Gough, C. M., Ivanov, V. Y., Jassal, R. S., Novick, K. A., Schafer, K. V. R., and Verbeeck, H.: Characterizing the diurnal patterns of errors in the prediction of evapotranspiration by several land-surface models: an NACP analysis, J. Geophys. Res., 119, 1458–1473, 2014. 8969
Max Planck Institute for Biogeochemistry: Eddy covariance gap-filling and flux-partitioning tool, available at: http://www.bgc-jena.mpg.de/~MDIwork/eddyproc/ (last access: June 2015), 2013. 8949
Miles, N. L., Richardson, S. J., Davis, K. J., Lauvaux, T., Andrews, A. E., West, T. O., Bandaru, V., and Crosson, E. R.: Large amplitude spatial and temporal gradients in atmospheric

BGD
12, 8939–9004, 2015

boundary layer CO_2 mole fractions detected with a tower-based network in the U.S. upper Midwest, J. Geophys. Res., 117, G01019, doi:10.1029/2011JG001781, 2012. 8957
Misson, L., Gershenson, A., Tang, J. W., McKay, M., Cheng, W. X., and Goldstein, A.: Influences of canopy photosynthesis and summer rain pulses on root dynamics and soil respiration in a young ponderosa pine forest, Tree Physiol., 26, 833–844, 2006. 8941
Misson, L., Baldocchi, D. D., Black, T. A., Blanken, P. D., Brunet, Y., Yuste, J. C., Dorsey, J. R., Falk, M., Granier, A., Irvine, M. R., Jarosz, N., Lamaud, E., Launiainen, S., Law, B. E., Longdoz, B., Loustau, D., Mckay, M., Paw, K. T., Vesala, T., Vickers, D., Wilson, K. B., and Goldstein, A. H.: Partitioning forest carbon fluxes with overstory and understory eddy-covariance measurements: a synthesis based on FLUXNET data, Agr. Forest Meteorol., 144, 14–31, 2007. 8943
Moene, A. F., and Van Dam, J. C.: Transport in the Atmosphere-Vegetation-Soil Continuum, Cambridge University Press, New York, 458 pp., doi:10.1017/CBO9781139043137, 2014. 8941
Moncrieff, J. B., Malhi, Y., and Leuning, R.: The propagation of errors in long-term measurements of land-atmosphere fluxes of carbon and water, Glob. Change Biol., 2, 231–240, 1996. 8972
Monson, R. K., Turnipseed, A. A., Sparks, J. P., Harley, P. C., Scott-Denton, L. E., Sparks, K., and Huxman, T. E.: Carbon sequestration in a high-elevation, subalpine forest, Glob. Change Biol., 8, 459–478, 2002. 8944, 8947, 8965, 8966, 8971
Monson, R. K., Sparks, J. P., Rosenstiel, T. N., Scott-Denton, L. E., Huxman, T. E., Harley, P. C., Turnipseed, A. A., Burns, S. P., Backlund, B., and Hu, J.: Climatic influences on net ecosystem CO_2 exchange during the transition from wintertime carbon source to springtime carbon sink in a high-elevation, subalpine forest, Oecologia, 146, 130–147, 2005. 8945, 8952
Monson, R. K., Prater, M. R., Hu, J., Burns, S. P., Sparks, J. P., Sparks, K. L., and Scott-Denton, L. E.: Tree species effects on ecosystem water-use efficiency in a high-elevation, subalpine forest, Oecologia, 162, 491–504, doi:10.1007/s00442-009-1465-z, 2010. 8945
Monteith, J. L.: Evaporation and environment, in: The State and Movement of Water in Living Organisms, edited by: Fogg, G. E., Academic Press, New York, 205–234, 1965. 8942, 8943
Monteith, J. L.: A reinterpretation of stomatal responses to humidity, Plant Cell Environ., 18, 357–364, 1995. 8943
Moore, D. J. P., Hu, J., Sacks, W. J., Schimel, D. S., and Monson, R. K.: Estimating transpiration and the sensitivity of carbon uptake to water availability in a subalpine forest using a simple

BGD
12, 8939–9004, 2015

ecosystem process model informed by measured net CO_2 and H_2O fluxes, Agr. Forest Meteorol., 148, 1467–1477, 2008. 8961
Munson, S. M., Benton, T. J., Lauenroth, W. K., and Burke, I. C.: Soil carbon flux following pulse precipitation events in the shortgrass steppe, Ecol. Res., 25, 205–211, 2010. 8941
Novick, K. A., Stoy, P. C., Katul, G. G., Ellsworth, D. S., Siqueira, M. B. S., Juang, J., and Oren, R.: Carbon dioxide and water vapor exchange in a warm temperate grassland, Oecologia, 138, 259–274, 2004. 8952
Novick, K. A., Oren, R., Stoy, P. C., Siqueira, M. B. S., and Katul, G. G.: Nocturnal evapotranspiration in eddy-covariance records from three co-located ecosystems in the Southeastern U.S.: implications for annual fluxes, Agr. Forest Meteorol., 149, 1491–1504, 2009. 8961
Oishi, A. C., Oren, R., and Stoy, P. C.: Estimating components of forest evapotranspiration: a footprint approach for scaling sap flux measurements, Agr. Forest Meteorol., 148, 1719–1732, 2008. 8943
Oliveira, P. E. S., Acevedo, O. C., Moraes, O. L. L., Zimermann, H. R., and Teichrieb, C.: Nocturnal intermittent coupling between the interior of a pine forest and the air above it, Bound.-Lay. Meteorol., 146, 45–64, 2013. 8952
Oncley, S. P., Foken, T., Vogt, R., Kohsiek, W., DeBruin, H. A. R., Bernhofer, C., Christen, A., van Gorsel, E., Grantz, D., Feigenwinter, C., Lehner, I., Liebethal, C., Liu, H., Mauder, M., Pitacco, A., Ribeiro, L., and Weidinger, T.: The Energy Balance Experiment EBEX-2000. Part I: Overview and energy balance, Bound.-Lay. Meteorol., 123, 1–28, 2007. 8946
Parrish, D. D., Hahn, C. H., Fahey, D. W., Williams, E. J., Bollinger, M. J., Hubler, G., Buhr, M. P., Murphy, P. C., Trainer, M., Hsie, E. Y., Liu, S. C., and Fehsenfeld, F. C.: Systematic variations in the concentration of NO_x (NO plus NO_2) at Niwot Ridge, Colorado, J. Geophys. Res., 95, 1817–1836, 1990. 8946
Parton, W., Morgan, J., Smith, D., Del Grosso, S., Prihodko, L., Lecain, D., Kelly, R., and Lutz, S.: Impact of precipitation dynamics on net ecosystem productivity, Glob. Change Biol., 18, 915–927, 2012. 8941, 8942
Pattantyús-Ábrahám, M., and Jánosi, I. M.: What determines the nocturnal cooling timescale at 2 m?, Geophys. Res. Lett., 31, L05109, doi:10.1029/2003GL019137, 2004. 8941
Penman, H. L.: Natural evaporation from open water, bare soil and grass, P. Roy. Soc. Lond. A Mat., 193, 120–145, doi:10.1098/rspa.1948.0037, 1948. 8942
Pino, D., Vilà-Guerau de Arellano, J., Peters, W., Schröter, J., van Heerwaarden, C. C., and Krol, M. C.: A conceptual framework to quantify the influence of convective boundary

BGD
12, 8939–9004, 2015

layer development on carbon dioxide mixing ratios, Atmos. Chem. Phys., 12, 2969–2985, doi:10.5194/acp-12-2969-2012, 2012. 8970

Polley, H. W., Emmerich, W., Bradford, J. A., Sims, P. L., Johnson, D. A., Sallendra, N. Z., Svejcar, T., Angell, R., Frank, A. B., Phillips, R. L., Snyder, K. A., Morgan, J. A., Sanabria, J., Mielnick, P. C., and Dugas, W. A.: Precipitation regulates the response of net ecosystem CO_2 exchange to environmental variation on United States Rangelands, Rangeland Ecol. Manag., 63, 176–186, 2010. 8943

Rana, G. and Katerji, N.: Measurement and estimation of actual evapotranspiration in the field under Mediterranean climate: a review, Eur. J. Agron., 13, 125–153, 2000. 8943

Rasmussen, R., Baker, B., Kochendorfer, J., Meyers, T., Landolt, S., Fischer, A. P., Black, J., Theriault, J. M., Kucera, P., Gochis, D., Smith, C., Nitu, R., Hall, M., Ikeda, K., and Gutmann, E.: How well are we measuring snow? The NOAA/FAA/NCAR Winter Precipitation Test Bed, B. Am. Meteorol. Soc., 93, 811–829, 2012. 8971

Reichstein, M., Falge, E., Baldocchi, D., Papale, D., Aubinet, M., Berbigier, P., Bernhofer, C., Buchmann, N., Gilmanov, T., Granier, A., Grunwald, T., Havrankova, K., Ilvesniemi, H., Janous, D., Knohl, A., Laurila, T., Lohila, A., Loustau, D., Matteucci, G., Meyers, T., Miglietta, F., Ourcival, J. M., Pumpanen, J., Rambal, S., Rotenberg, E., Sanz, M., Tenhunen, J., Seufert, G., Vaccari, F., Vesala, T., Yakir, D., and Valentini, R.: On the separation of net ecosystem exchange into assimilation and ecosystem respiration: review and improved algorithm, Glob. Change Biol., 11, 1424–1439, 2005. 8949, 8952

Riveros-Iregui, D. A., Hu, J., Burns, S. P., Bowling, D. R., and Monson, R. K.: An interannual assessment of the relationship between the stable carbon isotopic composition of ecosystem respiration and climate in a high-elevation subalpine forest, J. Geophys. Res., 116, G02005, doi:10.1029/2010JG001556, 2011. 8944

Ruimy, A., Jarvis, P. G., Baldocchi, D. D., and Saugier, B.: CO_2 fluxes over plant canopies and solar radiation: a review, Adv. Ecol. Res., 26, 1–68, 1995. 8966

Ryan, M. G. and Law, B.: Interpreting, measuring, and modeling soil respiration, Biogeochemistry, 73, 3–27, 2005. 8941

Sánchez-Cañete, E. P., Kowalski, A. S., Serrano-Ortiz, P., Pérez-Priego, O., and Domingo, F.: Deep CO_2 soil inhalation / exhalation induced by synoptic pressure changes and atmospheric tides in a carbonated semiarid steppe, Biogeosciences, 10, 6591–6600, doi:10.5194/bg-10-6591-2013, 2013. 8958

BGD
12, 8939–9004, 2015

Savage, K., Davidson, E. A., Richardson, A. D., and Hollinger, D. Y.: Three scales of temporal resolution from automated soil respiration measurements, Agr. Forest Meteorol., 149, 2012–2021, 2009. 8941

Scanlon, T. M. and Kustas, W. P.: Partitioning carbon dioxide and water vapor fluxes using correlation analysis, Agr. Forest Meteorol., 150, 89–99, 2010. 8943

Schaeffer, S. M., Anderson, D. E., Burns, S. P., Monson, R. K., Sun, J., and Bowling, D. R.: Canopy structure and atmospheric flows in relation to the $\delta^{13}C$ of respired CO_2 in a subalpine coniferous forest, Agr. Forest Meteorol., 148, 592–605, doi:10.1016/j.agrformet.2007.11.003, 2008a. 8949, 8958

Schaeffer, S. M., Miller, J. B., Vaughn, B. H., White, J. W. C., and Bowling, D. R.: Long-term field performance of a tunable diode laser absorption spectrometer for analysis of carbon isotopes of CO_2 in forest air, Atmos. Chem. Phys., 8, 5263–5277, doi:10.5194/acp-8-5263-2008, 2008b. 8971

Schlaepfer, D. R., Ewers, B. E., Shuman, B. N., Williams, D. G., Frank, J. M., Massman, W. J., and Lauenroth, W. K.: Terrestrial water fluxes dominated by transpiration: comment, Ecosphere, 5(5), 61, doi:10.1890/ES13-00391.1, 2014. 8962

Schmidt, A., Hanson, C., Chan, W. S., and Law, B. E.: Empirical assessment of uncertainties of meteorological parameters and turbulent fluxes in the AmeriFlux network, J. Geophys. Res., 117, G04014, doi:10.1029/2012JG002100, 2012. 8972

Schultz, D. M.: A review of cold fronts with prefrontal troughs and wind shifts, Mon. Weather Rev., 133, 2449–2472, 2005. 8957

Scott-Denton, L. E., Sparks, K. L., and Monson, R. K.: Spatial and temporal controls of soil respiration rate in a high-elevation, subalpine forest, Soil Biol. Biochem., 35, 525–534, 2003. 8945, 8964

Scott-Denton, L. E., Rosenstiel, T. N., and Monson, R. K.: Differential controls by climate and substrate over the heterotrophic and rhizospheric components of soil respiration, Glob. Change Biol., 12, 205–216, 2006. 8951, 8964

Staebler, R. M. and Fitzjarrald, D. R.: Observing subcanopy CO_2 advection, Agr. Forest Meteorol., 122, 139–156, 2004. 8964

Staudt, K., Serafimovich, A., Siebicke, L., Pyles, R. D., and Falge, E.: Vertical structure of evapotranspiration at a forest site (a case study), Agr. Forest Meteorol., 151, 709–729, 2011. 8943, 8962

BGD
12, 8939–9004, 2015

Stephens, B. B., Miles, N. L., Richardson, S. J., Watt, A. S., and Davis, K. J.: Atmospheric CO_2 monitoring with single-cell NDIR-based analyzers, Atmos. Meas. Tech., 4, 2737–2748, doi:10.5194/amt-4-2737-2011, 2011. 8957

Stoy, P. C., Katul, G. G., Siqueira, M. B. S., Juang, J. Y., Novick, K. A., Uebelherr, J. M., and Oren, R.: An evaluation of models for partitioning eddy covariance-measured net ecosystem exchange into photosynthesis and respiration, Agr. Forest Meteorol., 141, 2–18, 2006. 8949

Sun, J., Burns, S. P., Delany, A. C., Oncley, S. P., Turnipseed, A. A., Stephens, B. B., Lenschow, D. H., LeMone, M. A., Monson, R. K., and Anderson, D. E.: CO_2 transport over complex terrain, Agr. Forest Meteorol., 145, 1–21, doi:10.1016/j.agrformet.2007.02.007, 2007. 8966

Tang, J. W., Misson, L., Gershenson, A., Cheng, W. X., and Goldstein, A. H.: Continuous measurements of soil respiration with and without roots in a ponderosa pine plantation in the Sierra Nevada Mountains, Agr. Forest Meteorol., 132, 212–227, 2005. 8941

Thomas, C. K., Law, B. E., Irvine, J., Martin, J. G., Pettijohn, J. C., and Davis, K. J.: Seasonal hydrology explains interannual and seasonal variation in carbon and water exchange in a semiarid mature ponderosa pine forest in central Oregon, J. Geophys. Res., 114, G04006, doi:10.1029/2009JG001010, 2009. 8943

Thomas, C. K., Martin, J. G., Law, B. E., and Davis, K.: Toward biologically meaningful net carbon exchange estimates for tall, dense canopies: multi-level eddy covariance observations and canopy coupling regimes in a mature Douglas-fir forest in Oregon, Agr. Forest Meteorol., 173, 14–27, doi:10.1016/j.agrformet.2013.01.001, 2013. 8952, 8964

Turnipseed, A. A., Blanken, P. D., Anderson, D. E., and Monson, R. K.: Energy budget above a high-elevation subalpine forest in complex topography, Agr. Forest Meteorol., 110, 177–201, 2002. 8944, 8945, 8946, 8947, 8966, 8968

Turnipseed, A. A., Anderson, D. E., Blanken, P. D., Baugh, W. M., and Monson, R. K.: Airflows and turbulent flux measurements in mountainous terrain. Part 1: canopy and local effects, Agr. Forest Meteorol., 119, 1–21, 2003. 8947

Turnipseed, A. A., Anderson, D. E., Burns, S., Blanken, P. D., and Monson, R. K.: Airflows and turbulent flux measurements in mountainous terrain. Part 2: mesoscale effects, Agr. Forest Meteorol., 125, 187–205, 2004. 8946

Turnipseed, A. A., Burns, S. P., Moore, D. J. P., Hu, J., Guenther, A. B., and Monson, R. K.: Controls over ozone deposition to a high elevation subalpine forest, Agr. Forest Meteorol., 149, 1447–1459, doi:10.1016/j.agrformet.2009.04.001, 2009. 8944, 8948, 8961

BGD
12, 8939–9004, 2015

Unger, S., Maguas, C., Pereira, J. S., David, T. S., and Werner, C.: The influence of precipitation pulses on soil respiration – Assessing the "Birch effect" by stable carbon isotopes, Soil Biol. Biochem., 42, 1800–1810, 2010. 8942

van Heerwaarden, C. C., Vilà-Guerau de Arellano, J., Moene, A. F., and Holtslag, A. A. M.: Interactions between dry-air entrainment, surface evaporation and convective boundary-layer development, Q. J. Roy. Meteor. Soc., 135, 1277–1291, doi:10.1002/qj.431, 2009. 8943, 8970

van Heerwaarden, C. C., Vilà-Guerau de Arellano, J., Gounou, A., Couvreux, F., and Guichard, F.: Understanding the daily cycle of evapotranspiration: a new method to quantify the influence of forcings and feedbacks, J. Hydrometeorol., 11, 1405–1422, doi:10.1175/2010JHM1272.1, 2010. 8943

Vickers, D., Thomas, C., and Law, B. E.: Random and systematic CO_2 flux sampling errors for tower measurements over forests in the convective boundary layer, Agr. Forest Meteorol., 149, 73–83, 2009. 8964

Wang, K. C. and Dickinson, R. E.: A review of global terrestrial evapotranspiration: observation, modeling, climatology, and climatic variability, Rev. Geophys., 50, RG2005, doi:10.1029/2011RG000373, 2012. 8943

Wang, K. C., Dickinson, R. E., and Liang, S. L.: Observational evidence on the effects of clouds and aerosols on net ecosystem exchange and evapotranspiration, Geophys. Res. Lett., 35, L10401, doi:10.1029/2008GL034167, 2008. 8966

Werner, C., Schnyder, H., Cuntz, M., Keitel, C., Zeeman, M. J., Dawson, T. E., Badeck, F.-W., Brugnoli, E., Ghashghaie, J., Grams, T. E. E., Kayler, Z. E., Lakatos, M., Lee, X., Máguas, C., Ogée, J., Rascher, K. G., Siegwolf, R. T. W., Unger, S., Welker, J., Wingate, L., and Gessler, A.: Progress and challenges in using stable isotopes to trace plant carbon and water relations across scales, Biogeosciences, 9, 3083–3111, doi:10.5194/bg-9-3083-2012, 2012. 8943

Whiteman, C. D.: Mountain Meteorology: Fundamentals and Applications, Oxford University Press, New York, 355 pp., 2000. 8946, 8957

Williams, D. G., Cable, W., Hultine, K., Hoedjes, J. C. B., Yepez, E. A., Simonneaux, V., Er-Raki, S., Boulet, G., de Bruin, H. A. R., Chehbouni, A., Hartogensis, O. K., and Timouk, F.: Evapotranspiration components determined by stable isotope, sap flow and eddy covariance techniques, Agr. Forest Meteorol., 125, 241–258, 2004. 8943

BGD
12, 8939–9004, 2015

Williams, M. W., Losleben, M., Caine, N., and Greenland, D.: Changes in climate and hydrochemical responses in a high-elevation catchment in the Rocky Mountains, USA, Limnol. Oceanogr., 41, 939–946, 1996. 8971

Wilson, K. B., Hanson, P. J., Mulholland, P. J., Baldocchi, D. D., and Wullschleger, S. D.: A comparison of methods for determining forest evapotranspiration and its components: sap-flow, soil water budget, eddy covariance and catchment water balance, Agr. Forest Meteorol., 106, 153–168, 2001. 8943, 8962

Woods Hole Oceanographic Institution: SEA-MAT: Matlab Tools for Oceanographic Analysis, available at: http://woodshole.er.usgs.gov/operations/sea-mat/, last access: 26 December 2013. 8949

Xu, L. K., Baldocchi, D. D., and Tang, J. W.: How soil moisture, rain pulses, and growth alter the response of ecosystem respiration to temperature, Global Biogeochem. Cy., 18, GB4002, doi:10.1029/2004GB002281, 2004. 8941, 8942

Yakir, D. and Sternberg, L. d. L.: The use of stable isotopes to study ecosystem gas exchange, Oecologia, 123, 297–311, 2000. 8943

Yi, C., Anderson, D. E., Turnipseed, A. A., Burns, S. P., Sparks, J. P., Stannard, D. I., and Monson, R. K.: The contribution of advective fluxes to net ecosystem exchange in a high-elevation, subalpine forest, Ecol. Appl., 18, 1379–1390, doi:10.1890/06-0908.1, 2008. 8966

Zardi, D. and Whiteman, C. D.: Diurnal mountain wind systems, in: Mountain Weather Research and Forecasting, edited by: Chow, F. K., De Wekker, S. F. J., and Snyder, B. J., Springer Atmospheric Sciences, Springer, Dordrecht, the Netherlands, 35–119, doi:10.1007/978-94-007-4098-3_2, 2013. 8946

Zawadzki, I. I.: Statistical properties of precipitation patterns, J. Appl. Meteorol., 12, 459–472, 1973. 8948

Zobitz, J. M., Burns, S. P., Reichstein, M., and Bowling, D. R.: Partitioning net ecosystem carbon exchange and the carbon isotopic disequilibrium in a subalpine forest, Glob. Change Biol., 14, 1785–1800, doi:10.1111/j.1365-2486.2008.01609.x, 2008. 8949

BGD
12, 8939–9004, 2015

Table 1. Precipitation statistics for the US-NR1 AmeriFlux site. The number of days with a daily precipitation greater than 3 mm day^{-1} for each year and month is shown. These are defined as "wet" days in the analysis (see text for details). If the warm-season started in June, then the May column is filled with "NA". The total cumulative precipitation from the wet days is given immediately below the number of days. In the two right-hand columns the cumulative precipitation from the wet days only and from all days within the warm season are provided. Precipitation units are mm.

	Day of Year						Cumulative Precipitation	
Year	Start[a]	May	June	July	August	September	(Wet Days)	(Warm Season)
2012[b]	135	3	2	12	2	5	24	140
		25.0	10.5	214.0	13.5	58.8	321.8	353.2
2011[b]	168	NA	3	7	3	6	19	106
			49.9	72.5	27.8	56.6	206.8	230.6
2010	156	NA	4	7	6	1	18	118
			64.8	53.8	63.5	4.1	186.2	211.6
2009	153	NA	8	5	1	6	20	121
			54.6	38.1	3.6	37.6	133.9	175.9
2008	160	NA	0	6	10	4	20	115
				31.7	134.9	49.9	216.5	241.9
2007	160	NA	1	8	8	6	23	114
			10.7	74.9	57.9	32.8	176.3	211.5
2006	142	1	1	6	2	5	15	132
		10.9	3.6	120.9	13.0	54.9	203.2	245.6
2005	152	NA	9	3	7	4	23	122
			48.5	36.1	45.6	30.7	160.9	191.2
2004	138	1	11	6	7	6	31	137
		4.6	111.3	89.6	61.7	56.2	323.4	365.3

BGD
12, 8939–9004, 2015

Table 1. Continued.

Year	Day of Year Start[a]	May	June	July	August	September	Cumulative Precipitation (Wet Days)	Cumulative Precipitation (Warm Season)
2003	153	NA	4	6	6	4	20	121
			24.2	32.1	52.7	17.9	126.9	161.5
2002	137	2	3	5	6	6	22	137
		32.3	37.6	43.7	50.0	63.5	227.1	249.6
2001	142	2	4	7	7	4	24	132
		7.6	21.3	98.0	81.5	44.9	253.4	301.8
2000	142	2	6	4	6	6	24	133
		15.5	65.8	42.1	53.3	65.3	242.0	268.1
1999[c]	158	NA	4	5	8	6	23	116
			18.0	106.0	73.7	43.0	240.7	290.0
Total		11	60	87	79	69	306	1744
Mean	149.7	6.8	37.2	75.3	52.3	44.0	215.6	249.8

[a] This column indicates the day of year the warm season started based on diel changes in the soil temperature as shown in Fig. 1.

[b] For 2011 and 2012, precipitation from the NOAA U.S. Climate Reference Network (USCRN; Diamond et al., 2013) MRS "Hills Mills" station was used due to instrument problems with the tipping bucket at the AmeriFlux tower (see text for details).

[c] For 1999, precipitation from the LTER C-1 site was used.

BGD
12, 8939–9004, 2015

Table 2. Variables, symbols, units, and height above ground of measurements along with the number of days each variable falls within each precipitation category. Where appropriate, the percentage gap-filled 30 min data for each particular variable is shown. If any variable is missing for a 30 min period, then all variables within that particular group are excluded.

Variable	Symbol	Units	Sensor Height [cm]	Total Number of Days and Percentage of Gap-filled Values Dry1	Wet1	Wet2	Dry2	Notes
Measurements between 1999–2012				1209	194	99	199	
Net Radiation	R_{net}	$W\,m^{-2}$	2550	0.5 %	2.1 %	2.8 %	1.6 %	
Photosynthetically Active Radiation	PAR	$\mu mol\,m^{-2}\,s^{-1}$	2550	1.3 %	3.0 %	3.6 %	2.2 %	
Barometric Pressure	P	kPa	1050	1.1 %	3.4 %	3.6 %	2.2 %	
Air Temperature, Relative Humidity Specific Humidity	T_a, RH q	°C, percent $g\,kg^{-1}$	2150	0.6 %	2.3 %	2.9 %	1.5 %	
Soil Temperature	T_{soil}	°C	−5	3.5 %	3.5 %	4.3 %	4.7 %	**A**
Wind Speed, Wind Direction	U, WD	$m\,s^{-1}$, deg from true N	2150	1.7 %	5.8 %	11.0 %	3.2 %	**B**
Friction Velocity	u_*	$m\,s^{-1}$	2150	2.3 %	5.5 %	7.9 %	3.0 %	
Sensible Heat Flux	H	$W\,m^{-2}$	2150	6.0 %	15.8 %	29.1 %	10.9 %	
Latent Heat Flux	LE	$W\,m^{-2}$	2150	7.2 %	15.4 %	25.8 %	11.6 %	
Net Ecosystem Exchange of CO_2	NEE	$\mu mol\,m^{-2}\,s^{-1}$	2150	12.0 %	24.9 %	37.5 %	20.8 %	**C**

BGD
12, 8939–9004, 2015

Table 2. Continued.

Variable	Symbol	Units	Sensor Height [cm]	Total Number of Days and Percentage of Gap-filled Values Dry1	Wet1	Wet2	Dry2	Notes
Measurements between 2000–2012				1144	186	97	188	
Precipitation	Precip	mm (30 min)$^{-1}$	1050	3.8 %	2.8 %	3.0 %	1.5 %	**D**
Measurements between 2002–2012				924	148	76	148	
Volumetric Water Content	VWC	$m^3\,m^{-3}$	−5	0.01 %	0.01 %	0.01 %	0 %	**A**
Soil Heat Flux	G_z	W m^{-2}	−10	0.02 %	0.3 %	0.1 %	0.04 %	
Measurements between 2006–2012				530	83	46	82	
CO_2 Dry Mole Fraction	χ_c	µmol mol^{-1}	2150	37.3 % 10.7 %	34.8 % 6.5 %	35.8 % 6.2 %	37.3 % 8.0 %	**E**
Thermocouple Temperature	T_{tc}	°C	2198	6.6 %	2.3 %	1.0 %	2.2 %	

A: In October 2005, a soil moisture sensor (Campbell Scientific, model CS616) and soil temperature sensor (Campbell Scientific, model CS107) were installed horizontally at a depth of 5 cm within 50 m of the AmeriFlux tower. The CS107 thermistor was calibrated against a NIST-standard temperature sensor at the National Center for Atmospheric Research (NCAR) Integrated Surface Flux System (ISFS) calibration facility. These sensors were incorporated in the US-NR1 dataset starting in January 2006. Prior to this, an average of 5 soil temperature sensors (REBS, model STP-1) and 8 soil moisture sensors (Campbell Scientific, model CS615) were used to determine the soil properties. The CS615 sensors were inserted into the soil at a 45° angle providing an average moisture content over the upper 15 cm of the soil.
B: Whenver possible, U and WD were gap-filled with a prop-vane sensor at 25 m on US-NR1 tower. Otherwise, gap-filling was performed using U and WD from the LTER C-1 climate station (as described in Appendix A1) which have been adjusted to US-NR1 winds using a linear relationship.
C: NEE includes both the u_* filter and storage term gap-filling. The flux data have been screened such that around 2 % of the extreme values have been removed.
D: Gap-filling for the Met One tipping bucket on the US-NR1 tower is shown. The gap-filling flags for precipitation were incorrect prior to year 2003. Therefore, the gap-filling values listed here are for years 2003–2010. After year 2010, USCRN data were used (see Appendix A1 for details).
E: Between years 2008 to 2010, the CO_2 was sampled hourly rather than half-hourly. During periods with hourly measurements a linear interpolation was used to create data with half-hourly time stamps. The upper values shows the number of 30 min values missing prior to interpolation, while the lower numbers shows the number of missing values after interpolation.

BGD
12, 8939–9004, 2015

Table 3. Daytime and nighttime statistics of selected variables for different precipitation conditions.

Variable	Symbol	Sensor Height [cm]	Night (00:00–04:00 MST) Dry1	Wet1	Wet2	Dry2	Daytime (10:00–14:00 MST) Dry1	Wet1	Wet2	Dry2	Evening (19:00–23:00 MST) Dry1	Wet2	Wet2	Dry2
Primary Measurements														
Precipitation	Precip	1050	0.002	0.017	0.201	0.010	0.007	0.288	0.401	0.018	0.006	0.264	0.213	0.008
Net Radiation	R_{net}	2550	−71.7	−53.0	−33.3	−52.2	582.2	349.3	286.8	528.2	−64.7	−29.7	−30.3	−55.5
Photosynthetically Active Radiation	PAR	2550	0	0	0	0	1408.4	865.6	715.8	1273.4	0	0	0	0
Barometric Pressure	P	1050	70.97	70.92	70.93	70.97	70.97	70.92	70.93	70.97	70.97	70.92	70.93	70.97
Air Temperature	T_a	2150	10.0	9.7	7.0	7.3	14.8	11.7	8.9	11.9	11.1	7.8	6.8	9.3
		200	5.7	6.6	4.8	4.1	17.1	13.0	9.4	13.2	8.4	6.1	5.3	6.8
Thermocouple Temperature	T_{tc}	2198	10.2	10.1	7.6	7.7	15.5	12.3	9.0	12.9	11.4	8.2	6.8	9.5
		40	5.6	6.7	5.1	4.2	17.2	13.2	8.9	13.1	8.3	6.2	5.5	6.9
Vertical Difference	ΔT_{tc}	(2198 – 40)	4.65	3.46	2.46	3.45	−1.69	−0.87	0.11	−0.21	3.04	1.98	1.31	2.57
Soil Temperature	T_{soil}	−5	6.8	7.4	6.9	6.4	9.6	9.2	8.1	8.7	8.4	7.8	7.4	8.0
Soil Heat Flux	G_z	−10	−5.6	−4.2	−4.6	−5.5	17.0	11.5	7.4	15.3	−2.6	−3.1	−3.2	−2.9
Volumetric Water Content	VWC	−5	0.118	0.122	0.149	0.144	0.115	0.121	0.153	0.140	0.115	0.133	0.163	0.140
Wind Speed	U	2150	3.8	3.4	3.0	3.7	3.8	3.1	2.8	3.5	3.2	3.2	2.7	3.1
CO_2 Dry Mole Fraction	χ_c	2150	389.9	390.8	392.7	390.6	385.3	386.8	387.1	386.0	390.5	391.2	392.4	391.5
		100	424.1	425.8	426.8	421.9	388.8	391.9	395.2	391.6	421.9	415.0	417.7	423.5
		10	434.0	437.4	438.7	432.0	394.2	400.1	405.0	400.0	433.8	426.0	429.5	437.6
Vertical Difference	$\Delta\chi_c$	(2150 – 10)	−44.12	−46.58	−45.96	−41.42	−8.84	−13.32	−17.96	−13.94	−43.31	−34.81	−37.05	−46.11
Calculated Variables														
Specific Humidity	q	2150	4.9	6.2	7.0	6.4	5.2	7.4	7.9	6.6	5.5	7.4	7.3	6.5
		200	5.4	6.5	7.4	6.8	5.7	8.0	8.7	7.6	6.0	7.9	7.6	7.0
Vapor Pressure Deficit	VPD	800	0.7	0.54	0.25	0.34	1.1	0.61	0.31	0.71	0.74	0.28	0.20	0.47
Friction Velocity	u_*	2150	0.40	0.38	0.34	0.41	0.70	0.55	0.47	0.63	0.33	0.37	0.31	0.33
Bulk Richardson Number	Ri_b		0.31	0.22	0.14	0.21	−0.13	−0.12	−0.08	−0.09	0.24	0.09	0.11	0.22
Sensible Heat Flux	H	2150	−48.9	−39.2	−38.6	−54.0	278.6	146.4	84.8	200.8	−35.5	−43.0	−33.0	−33.6
Latent Heat Flux	LE	2150	9.1	8.6	17.4	22.7	169.7	123.1	118.2	192.4	9.2	24.7	18.4	12.5
Net Ecosystem Exchange	NEE	2150	2.5	2.6	2.6	2.5	−7.9	−6.6	−5.6	−8.5	3.0	2.9	2.8	2.9

BGD
12, 8939–9004, 2015

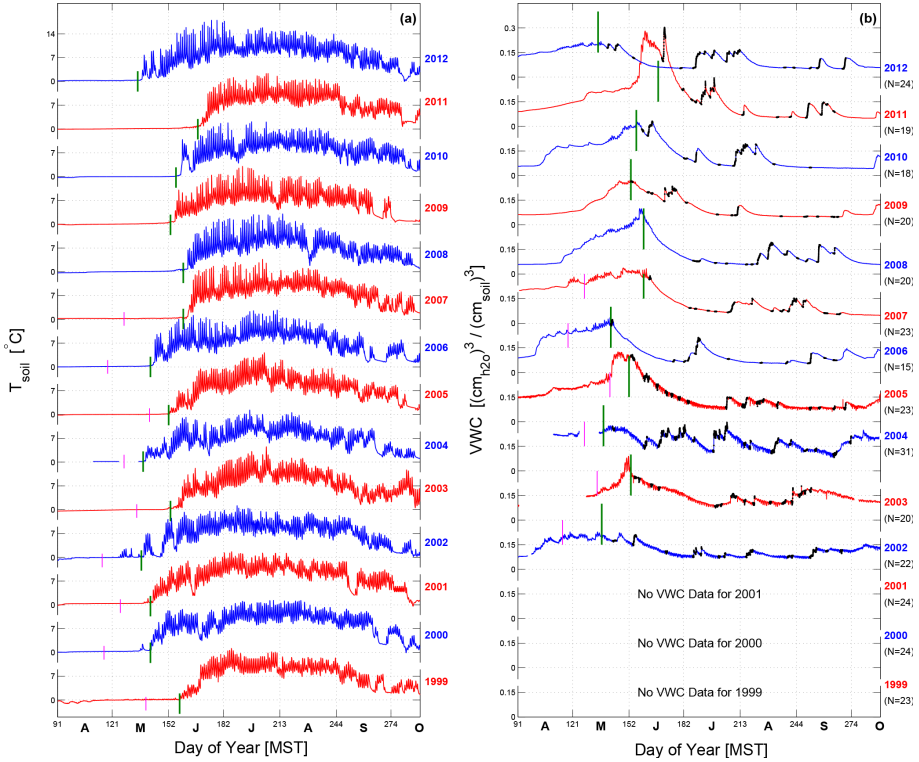

Figure 1. (a) Soil temperature and **(b)** soil moisture for years 1999 to 2012. In **(b)**, the black dots indicate wet days and the number of wet days for each year is shown to the right of the panel underneath the year. The warm-season start date was chosen based on the date that the soil temperature diurnal changes started to occur as indicated by the vertical green lines. The vertical mauve lines for years 1999–2007 are the start date of the growing season as determined by Hu et al. (2010a). Starting with year 2006, a single set of soil sensors at a depth of 5 cm were used (see Table 2 for details).

BGD
12, 8939–9004, 2015

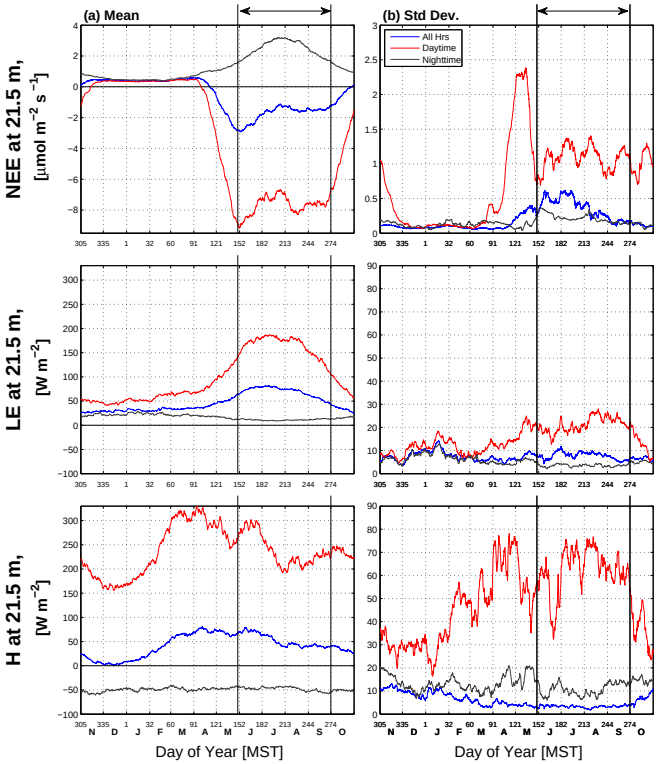

Figure 2. Fourteen-year **(a)** mean and **(b)** interannual standard deviation (n = 14 years) of (top) CO_2 net ecosystem exchange NEE, (middle) latent heat flux LE, and (bottom) sensible heat flux H. To remove the effects of short-term changes due to weather each 30 min yearly time series is averaged with a 20 day mean sliding window. In all panels, the statistics are calculated for all hours, daytime (10:00–14:00 MST), and nighttime (00:00–04:00 MST) periods following the legend in **(b)**. These data were collected between 1 November 1998 and 31 October 2012. Vertical lines with the arrows indicate the average warm-season period used for our study.

BGD
12, 8939–9004, 2015

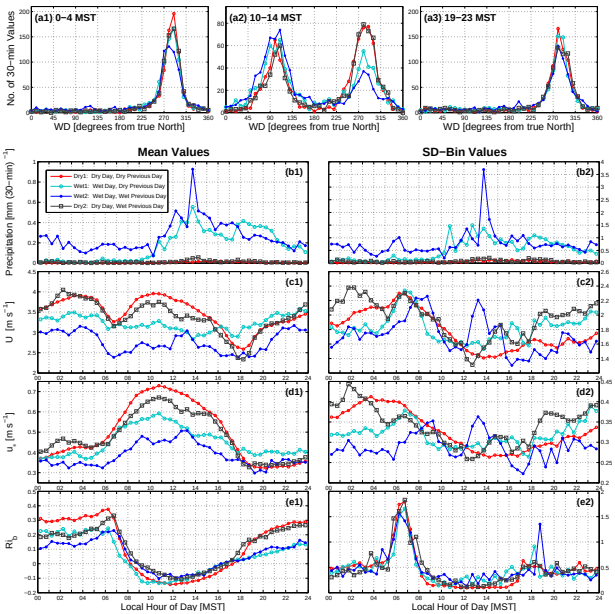

Figure 3. Frequency distributions of wind direction WD for different precipitation states for **(a1)** nighttime (00:00–04:00 MST) **(a2)** mid-day (10:00–14:00 MST), and **(a3)** late evening (19:00–23:00 MST) periods. Because there are a different number of 30 min periods within each precipitation state, the frequency distributions were created by randomly selecting 800 values for each precipitation state. Below **(a1–a3)**, the mean (left column) and standard deviation (SD-Bin, right column) of the warm-season diel cycle of **(b1, b2)** precipitation, **(c1, c2)** horizontal wind speed U at 21.5 m, **(d1, d2)** friction velocity u_*, and **(e1, e2)** bulk Richardson number Ri_b are shown. SD-Bin represents the amount of day-to-day variability within the diel cycle. These composites are from 30 min data during the warm-season between years 1999–2012. For all panels, each line represents a different precipitation state as shown in the legend of panel **(b1)**.

BGD
12, 8939–9004, 2015

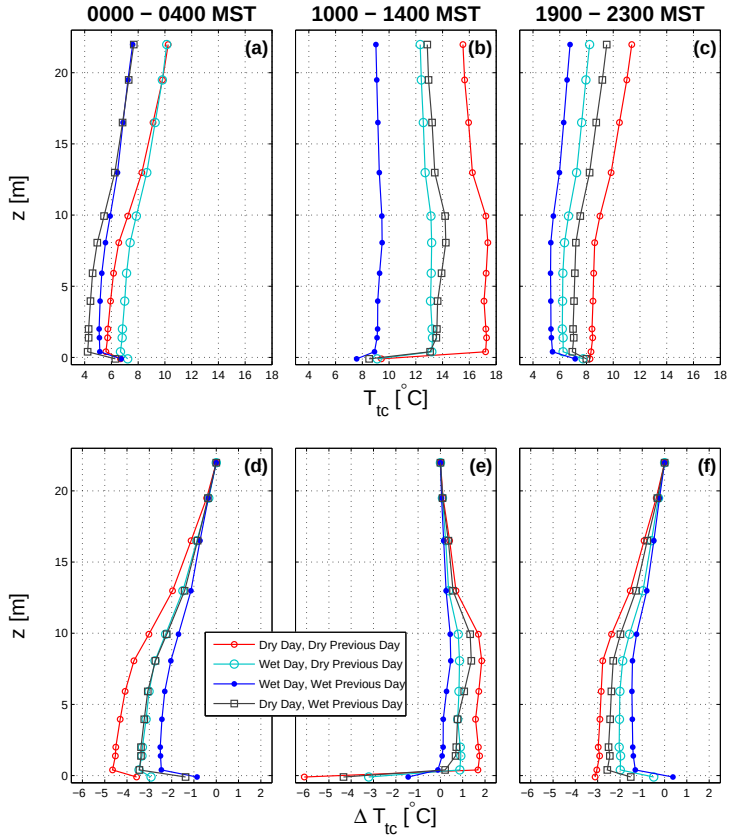

Figure 4. Vertical profiles of mean warm-season thermocouple air temperature T_{tc} for (left) nighttime (00:00–04:00 MST), (middle) mid-day (10:00–14:00 MST), and (right) late evening (19:00–23:00 MST). The upper row is the absolute T_{tc} while the bottom row is the T_{tc} difference relative to the highest level (21.98 m). Each line represents a different precipitation state as shown in the legend. These measurements are from the warm-season in years 2006–2012.

BGD
12, 8939–9004, 2015

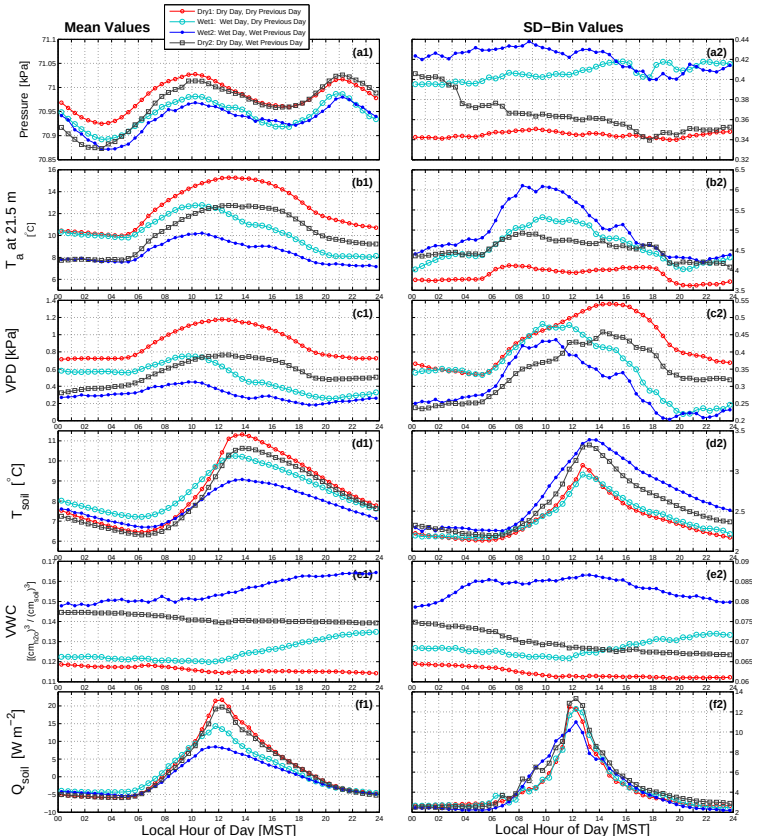

Figure 5. The mean (left column) and standard deviation (SD-Bin, right column) of the warm-season diel cycle of **(a1, a2)** barometric pressure, **(b1, b2)** air temperature T_a at 21.5 m, **(c1, c2)** vapor pressure deficit VPD, **(d1, d2)** soil temperature T_{soil}, **(e1, e2)** soil moisture VWC, and **(f1, f2)** soil heat flux Q_{soil}. SD-Bin represents the amount of day-to-day variability in the diel cycle. Each line represents a different precipitation state as shown in the legend.

BGD
12, 8939–9004, 2015

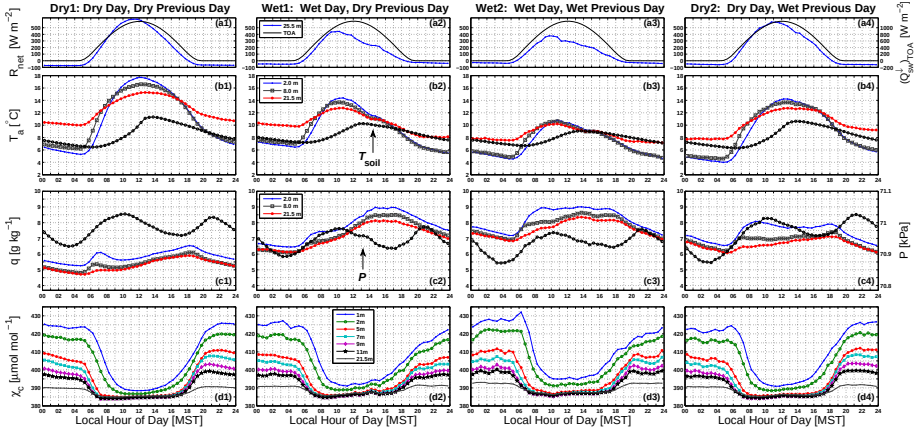

Figure 6. The warm-season mean diel cycle of: **(a1–a4)** net radiation R_{net}, **(b1–b4)** air and soil temperature T_a, T_{soil}, **(c1–c4)** specific humidity q and barometric pressure P, and **(d1–d4)** CO_2 mole fraction χ_c. Within each column the data are separated into diel periods based on whether significant rain occurred on that day. A "wet" day has a total daily precipitation of at least 3 mm (see text for further details). The legend in the 2nd column applies to all panels within each row.

BGD
12, 8939–9004, 2015

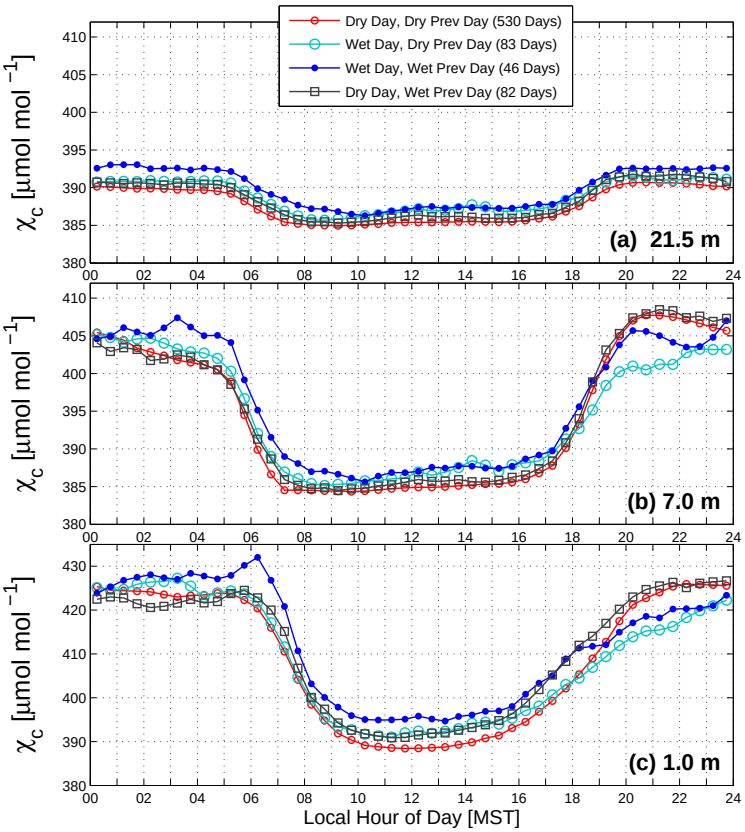

Figure 7. The warm-season mean diel cycle of CO_2 mole fraction χ_c at three different heights above the ground. Each line represents a different precipitation state as shown in the legend. These measurements are from the warm-season in years 2006–2012.

BGD
12, 8939–9004, 2015

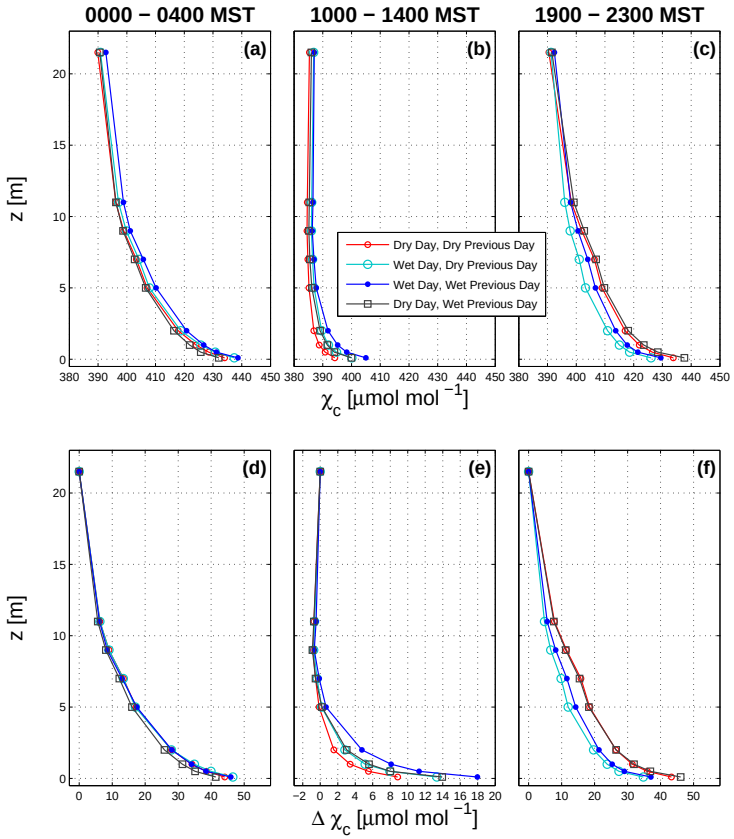

Figure 8. Mean vertical profiles of CO_2 mole fraction χ_c for (left) nighttime (00:00–04:00 MST), (middle) mid-day (10:00–14:00 MST), and (right) late evening (19:00–23:00 MST). The upper row is absolute χ_c while the bottom row is the χ_c difference relative to the highest level (21.5 m). Each line represents a different precipitation state as shown in the legend. These measurements are from the warm-season in years 2006–2012.

BGD
12, 8939–9004, 2015

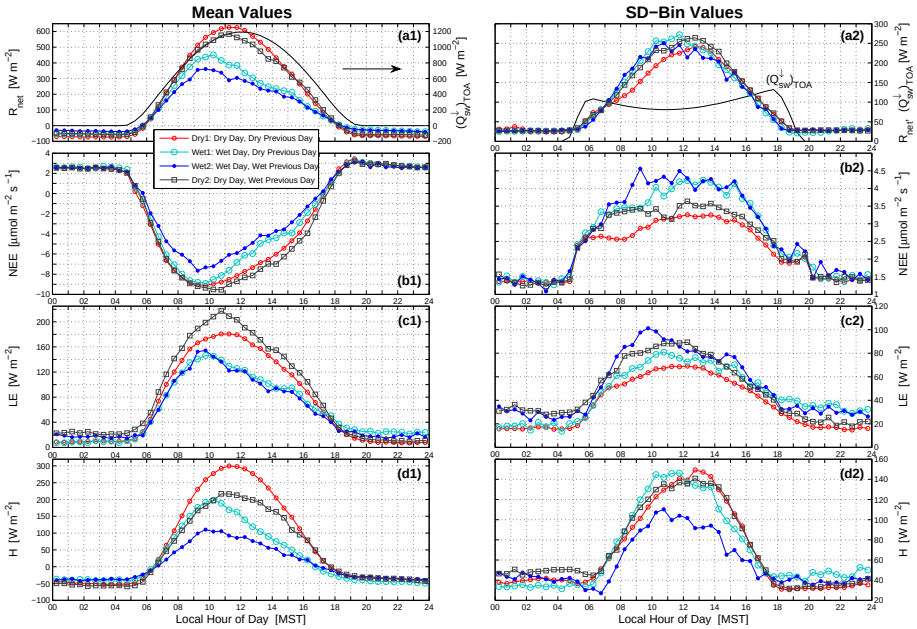

Figure 9. The mean (left column) and standard deviation (SD-Bin, right column) of the warm-season diel cycle of **(a1, a2)** net radiation R_{net}, **(b1, b2)** net ecosystem exchange of CO_2 NEE, **(c1, c2)** latent heat flux LE, and **(d1, d2)** sensible heat flux H. Each line represents a different precipitation state as shown in the legend. In **(a1, a2)**, incoming shortwave radiation at the top of the atmosphere $(Q^{\downarrow}_{SW})_{TOA}$ is shown as a black line (using the right-hand axes in **a1**). The diel cycle is calculated from 30 min measurements between years 1999–2012.

BGD
12, 8939–9004, 2015

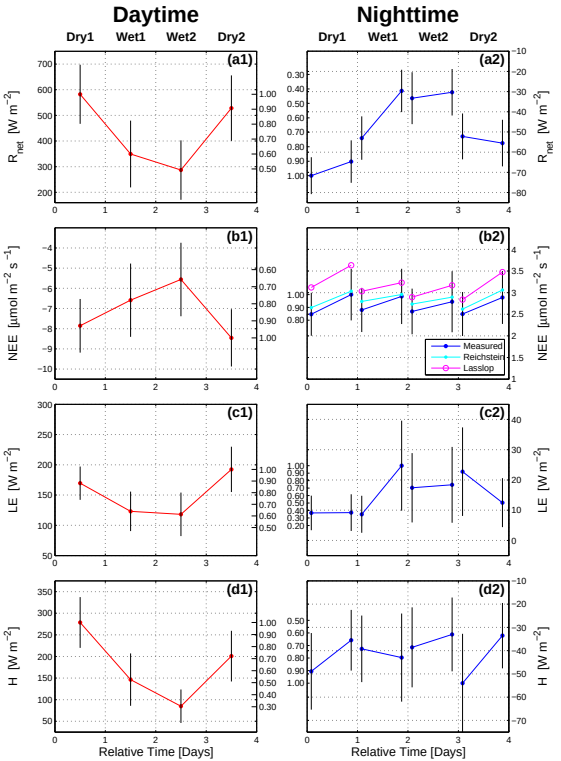

Figure 10. Mean values for (left side) daytime (10:00–14:00 MST) and (right side) night (00:00–04:00 MST) and evening (19:00–23:00 MST) periods of: **(a1, a2)** net radiation R_{net}; **(b1, b2)** net ecosystem exchange of CO_2 NEE; **(c1, c2)** latent heat flux LE; and **(d1, d2)** sensible heat flux H. The values are arranged from left-to-right in the order of Dry1, Wet1, Wet2, and Dry2 conditions. The vertical black lines represent the mean absolute deviation (MAD) of the 30 min data within that particular category and time period. The numerical values shown between the daytime and nighttime panels represent the fractional change relative to the largest (or smallest) data value within the panel.

BGD
12, 8939–9004, 2015

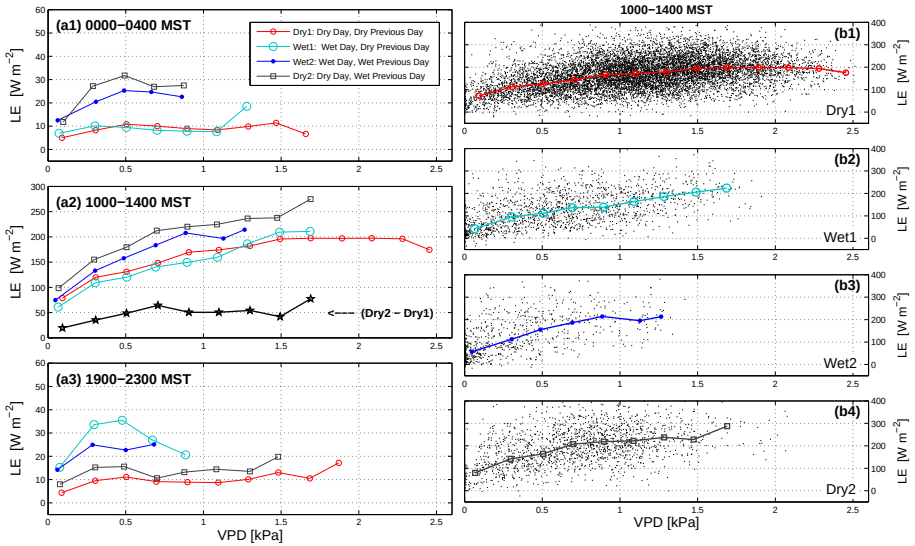

Figure 11. The (left column) binned 21.5 m latent heat flux LE vs. 8 m vapor pressure deficit VPD for **(a1)** night (00:00–04:00 MST), **(a2)** daytime (10:00–14:00 MST), and **(a3)** evening (19:00–23:00 MST) periods. Each line represents a different precipitation state as shown in the legend. In **(a2)**, the difference in LE between Dry2 and Dry1 conditions is shown as a black line. As an example of the variability in the binned data, the right-column panels show the 30 min daytime data used to create the binned daytime lines (i.e., corresponding to what is shown in panel **a2**) where the right-column panels are for **(b1)** Dry1, **(b2)** Wet1, **(b3)** Wet2, and **(b4)** Dry2 periods.

BGD
12, 8939–9004, 2015

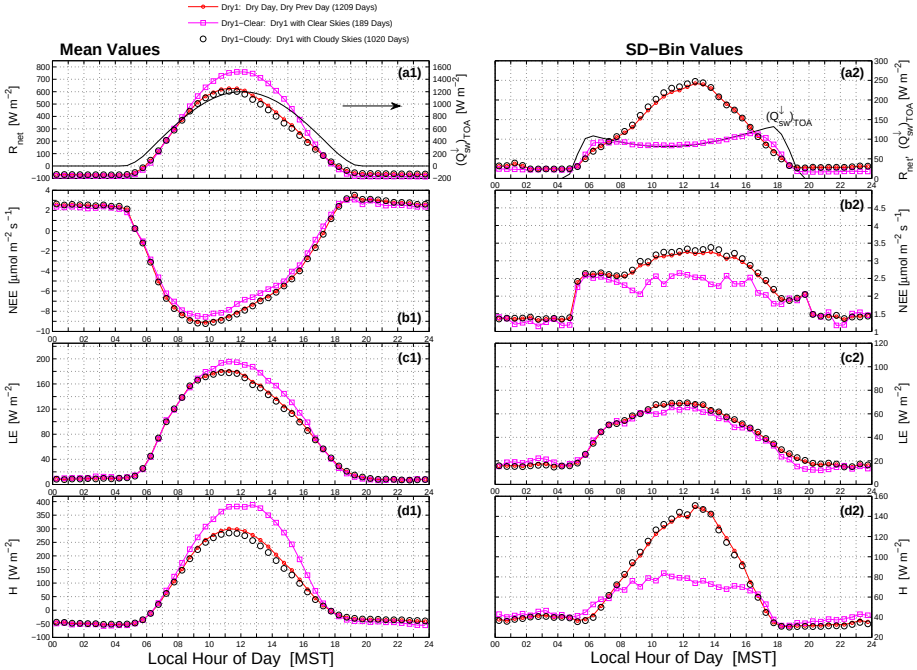

Figure 12. Similar to Fig. 9, except only Dry1 conditions are shown where the data have been further separated into Dry1-Clear and Dry1-Cloudy conditions as specified by the legend. For further details see the caption of Fig. 9.

BGD
12, 8939–9004, 2015

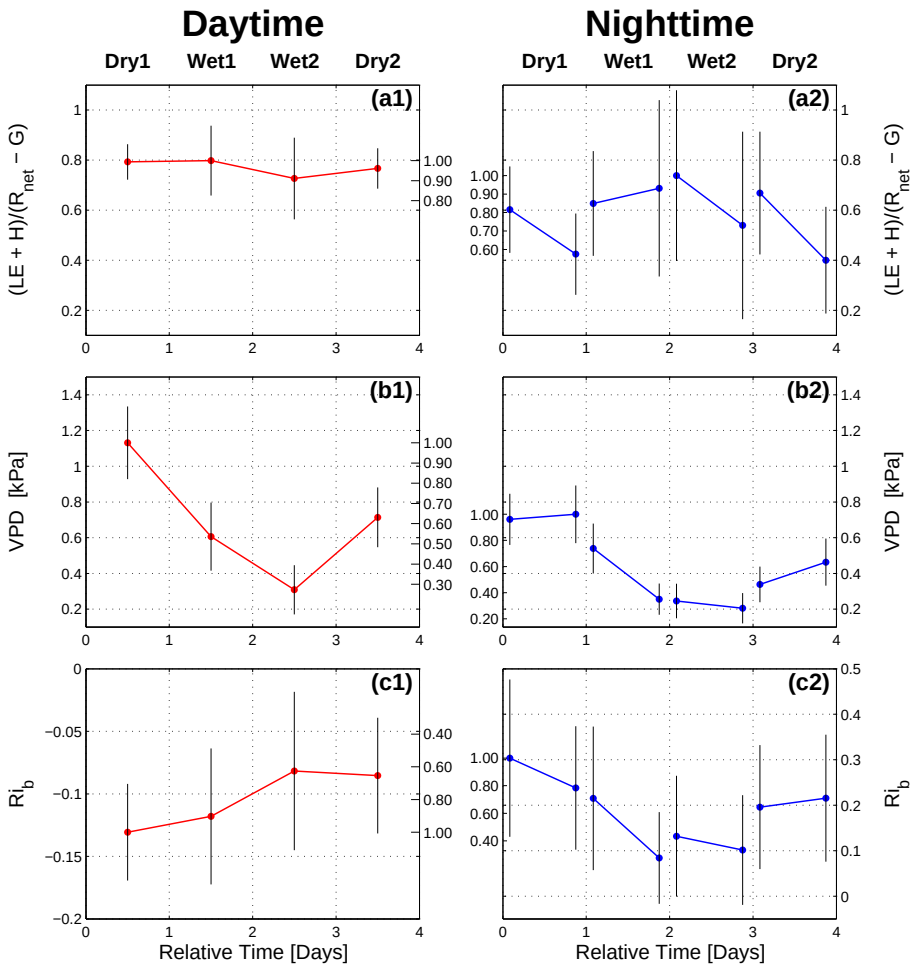

Figure 13. As in Fig. 10, showing **(a1, a2)** the surface energy balance closure fraction (LE + H)/($R_{net} - G$); **(b1, b2)** vapor pressure deficit VPD; and **(c1, c2)** bulk Richardson number Ri_b.

BGD
12, 8939–9004, 2015